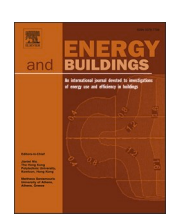
ELSEVIER

Contents lists available at ScienceDirect

Energy & Buildings

journal homepage: www.elsevier.com/locate/enb



Ultra-low temperature heating system based on dual-source solar assisted heat pump using compound parabolic concentrator-capillary tube solar collector

Li Wei Yang ^{a,c}, Jin Huan Pu ^{b,c,*}, Rong Ji Xu ^d, Tong Yang ^e, Hua Sheng Wang ^c

- ^a School of Energy and Power Engineering, Beihang University, 37 Xue Yuan Road, Beijing 100191, PR China
- ^b Institute for Advanced Technology, Shandong University, Jinan, Shandong 250061, PR China
- ^c School of Engineering and Materials Science, Queen Mary University of London, Mile End Road, London E1 4NS, UK
- ^d Beijing University of Civil Engineering and Architecture, Beijing 100044, PR China
- ^e Faculty of Science and Technology, Middlesex University, London NW4 4BT, UK

ARTICLEINFO

Keywords: Low temperature heating Compound parabolic concentrator-capillary tube solar collector Solar assisted air source heat pump

Domestic heating Seasonal performance factor

ABSTRACT

The fifth-generation heating – ultra-low temperature heating benefits to reduce electricity consumption and achieve the net zero goal. The dual-source solar assisted heat pump based heating system has been demonstrated to be an attractive green heating technology for the domestic sector. However, the slower response speed of the low temperature heating to the variation of heating load in responding to the variations of weather conditions limits its thermal comfort performance. The enhancement in solar collector performance brings valuable improvements in response speed of the heating system. In the present work, a heating system based on solar assisted air source heat pump using a compound parabolic concentrator-capillary tube solar collector (CPC-CSC) is investigated with the set heating temperatures of 40, 45, 50, and 55 °C. This heating system works for both space heating and hot water under the weather conditions in London. The results suggest that using a concentrated solar collector improves the response speed of the heating system at low set heating temperatures. For such a heating system, the ultra-low heating temperature increases the application of renewable energy and passive heating (by 6.4%). Compared with the dual-source indirect expansion solar assisted heat pump using flat plate collector, the heating system using CPC-CSC can reduce TEWI by 4.6% with a slightly longer (1.9%) payback period. As the set heating temperature decreases from 55 to 40 °C, the seasonal and yearly system seasonal performance factors significantly increase by 17.1% and 20.5%, respectively.

1. Introduction

Low temperature heating system refers to heating system providing hot water at a temperature within 45 °C [1]. The concept of low temperature heating has been widely adopted for district heating [2] and is strongly urged for decarbonisation in the heating sector [3]. For distributed heating, Kilkis [4] highlighted the benefits of low temperature heating in technology, environment and economic terms. Heat pump (HP) is a promising distributed heating technology to introduce low temperature heating to the domestic sector [5]. It can be combined with solar energy [6], i.e., solar assisted air source heat pump (SAASHP), for better system efficiency [7]. SAASHP can be divided into direct expansion type (DX-SAASHP) and indirect expansion type (IX-SAASHP) by expansion type; and can also be divided into serial, parallel and dual

source types according to the arrangement of heat sources. According to a review from Yang et al. [8], IX-SAASHP has more application potential for both space heating (SH) and hot water (HW). Simulation results from Yang et al. [9] suggested the possibility of applying parallel and dual-source IX-SAASHP for UK weather conditions.

Current research on low temperature heating mainly focuses on district heating while attention to distributed heating, especially SAASHP heating systems, is insufficient. Kaygusuz [10] conducted experiments and theoretical analyses on a serial-parallel IX-SAASHP with condensing temperatures of $40{\text -}55\,^{\circ}\text{C}$. The system obtained coefficient of performance (COP) of 4 in serial mode and 3 in parallel mode. Yerdash et al. [11] studied a solar assisted cascade HP using different refrigerant pairs. The system has a condensing temperature of $40{\text -}60\,^{\circ}\text{C}$ and COP of $1.8{\text -}3$. Qiu et al. [12] analysed a cascade serial IX-SAASHP and two kinds of two-stage dual-source DX-SAASHP. The condensing

E-mail address: j.pu@sdu.edu.cn (J.H. Pu).

 $^{^{\}ast}$ Corresponding author.

A collector area COP coefficient of performance Q_{HP} thermal energy obtained at the condenser of a heat pump Q_{HW} thermal energy for hot water Q_{loss} , SC heat loss from solar collector Q_{loss} linear heat loss from solar collector Q_{SC} thermal energy obtained by solar collector Q_{SH} thermal energy for space heating Q_{Su} solar energy used Q_{Su} solar energy supply Q_{TES} thermal energy storage I local solar irradiance for the tilted surface SF solar fraction SPF_{HP} seasonal performance factor of the heat pump SPF_{SyS} seasonal performance factor of the system T_{indoor} indoor air temperature T_{Indoor} indoor actual heating temperature (hot water temperature at the	oot numn
outlet of TES tank 2) TRNSYS TRaNsient System Simulation $T_{\rm HWS}^{\star}$ set heating temperature	ntrator-capillary tube solar ssisted air source heat pump eat pump assisted air source heat pump at pump

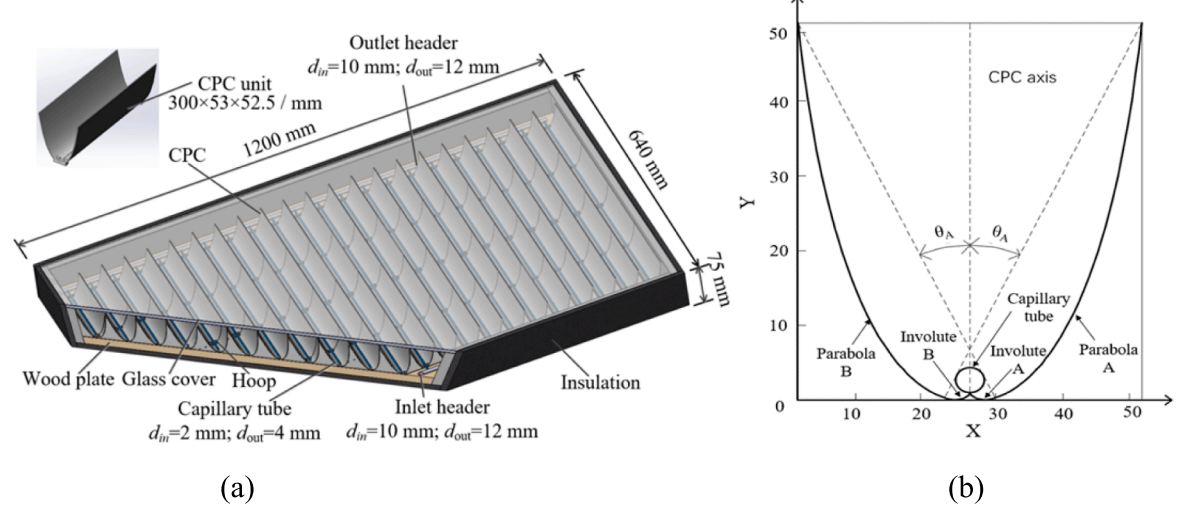


Fig. 1. Schematic of CPC-CSC: (a) 3D model (b) 2D model [19].

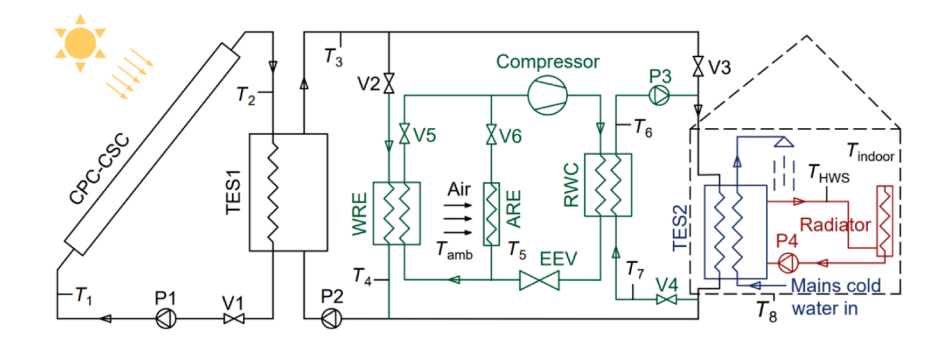
Table 1 Summary of experimental conditions.

	Solar irradiance, W/ m ²	Ambient air temperature, K	Air velocity, m/s	Date of experiments
1	290–1000	288–291	1–2	10 Oct. 2016—20 Nov. 2016
2	920–1000	289–293	1–2	5 Apr. 2017—10 May 2017

temperature of the systems was 50 °C and the COP is 2–2.9. Yang et al. [13] numerically simulated a dual-source IX-SAASHP with hot water supply temperatures of 40–55 °C for UK weather conditions where seasonal performance factor (SPF) can reach 5.0. Though low-temperature heating shows potential to achieve a higher system

efficiency, its low response speed to heating load limits its thermal comfort performance.

Innovation in system components, such as solar collectors, is a promising method to improve system operation performance. In addition to the commonly used flat plate solar collector (FPC), many kinds of advanced solar collectors have been designed and adopted for SAASHP, such as evacuated tube solar collectors [14], heat pipe solar collectors [15], solar roof [16], air-type solar collector [17] and compound parabolic concentrator (CPC) solar collector [18]. However, few studies have been conducted to use advanced collectors to improve low temperature heating. Among the advanced solar collectors, CPC collectors help to overcome the limit of solar availability and obtain higher water temperature as it can concentrate indirect incidence to the absorber, performing the possibility to make up the thermal comfort performance of ultra-low heating. Our research group [19] has proposed a CPC-capillary tube solar collector (CSC) whose collection efficiency is superior to those



Seven loops in the heating system:

(1) Solar collector loop: SC-TES1-V1-PA-SC

(2) TES1-WRE loop: TES1-V2-WRE-P2-TES1

(3) ASHP loop: ARE-V6-Compressor-RWC-EEV-ARE

(4) Space heating loop: TES2-Radiator-P4-TES2

(5) TES1-TES2 loop: TES1-V3-TES2-P2-TES1

(6) RWC-TES2 loop: RWC-P3-TES2-V4-RWC

(7) SWHP loop: WRE-V5-Compressor-RWC-EEV-WRE

SC: Solar collector

TES 1, TES 2: TES tank

V1 - V6: Valve

P1 - P4: Water pump

WRE: Water-to-refrigerant evaporator

ARE: Air-to-refrigerant evaporator

RWC: Refrigerant-to-water condenser

EEV: Expansion valve

 $T_1 - T_8$: Temperature sensor

Fig. 2. Schematic of the DSSAHP system [21].

 Table 2

 modules used in the DSSAHP model in TRNSYS.

Component	Module	Parameter	Value
CPC-CSC	Type 219	Collector area	8 m ²
	(self-	Inclination	51.5°
	established)	angle	_
FPC	Type 1b	Collector area	8 m ²
		Inclination angle	51.5°
		Tested flow rate	30 kg/hm2
		Intercept efficiency	0.8
		Efficiency slope	13 kJ/hm2k
		Efficiency	0 kJ/hm2k2
		curvature	
TES tank 1	Type 4a	Heat loss	$0.2 \text{ W/(m}^2 \text{ K)}$
		coefficient	
		Volume	500 L
		Height	1.175 m
TES tank 2	Type 4a	Heat loss	$0.2 \text{ W/(m}^2 \text{ K)}$
		coefficient	
		Volume	300 L
		Height	1 m
ASHP	Type 941	Blower power	0.15 kW
		Total air flow	1500 l/s
		rate	
		User defined file	YVAS012, York, Jonson
			Control
SWHP	Type 668	User defined file	30HXC-HP2, Carrier United
			Technologies

of other CPC collectors. In this research, the CPC-CSC is further applied in SAASHP heating system for low temperature heating.

This paper aims to investigate the operation performance for low temperature heating of a dual-source indirect expansion solar assisted heat pump (DSSAHP) using CPC-CSC. This system provides space heating and hot water for a single family house (SFH) 45 building under the weather conditions in London. The set heating temperature ($T_{\rm HWS}^*$) is set to be 40 °C, 45 °C, 50 °C and 55 °C to represent the applications of low temperature heating (40 °C and 45 °C cases) and normal heating

 $(50\,^{\circ}\text{C}\text{ and }55\,^{\circ}\text{C}\text{ cases})$. To evaluate the advantage of using CPC-CSC on low temperature heating, the operation performance of the system using FPC under the same working conditions is also analysed for comparison.

2. Compound parabolic concentrator-capillary solar collector

CPC-CSC is composed of CPC concentrators, absorbers (capillary tubes), headers, cover and insulation, as Fig. 1(a) shows [19]. The schematic of the CPC concentrators is shown in Fig. 1(b). The geometry of the CPC concentrators is determined by the principle of edge optics to concentrate solar incidence onto the receiver. The groove depth of the CPC is 52.5 mm and the aperture is 53 mm. The outer diameter of the absorber is 4 mm, equal to the diameter of the involute circle for CPC. This can ensure all the reflection of the solar radiation to be concentrated on the capillary tube. The inner diameter of the capillary tube is 2 mm. The concentrating ratio of CPC is 4.22 and the acceptance angle is 13.7° .

2.1. Numerical simulation and verification

The CPC-CSC is numerically simulated by ANSYS Fluent using a 3-D model. The computation domain is selected to be one CPC unit to represent the whole collector. The length of the CPC unit is 600 mm, the width is 53 mm, the height is 75 mm and the area is 0.0318 m². Water is adopted to be the fluid inside the capillary tube. The CPC-CSC is assumed to be in an open environment and thus convective heat transfers on cover and bottom are considered. The solar collection process combines conduction, convection, and radiation heat transfer. Convective heat transfer occurs between the outer wall of the capillary tubes and the air layer. The water flow inside the tubes is regarded as a 3D, steady, constant-property, laminar flow. Since the diameter of the copper capillary tubes is small compared with the size of CPCs, they are regarded as a homogeneous body heat source. All the surface temperatures of solid components are obtained from the coupled numerical simulations of air convection inside the collector, water flowing inside the capillary tubes and heat conduction in the solids.

Corresponding experiments were undertaken in Beijing, China. The

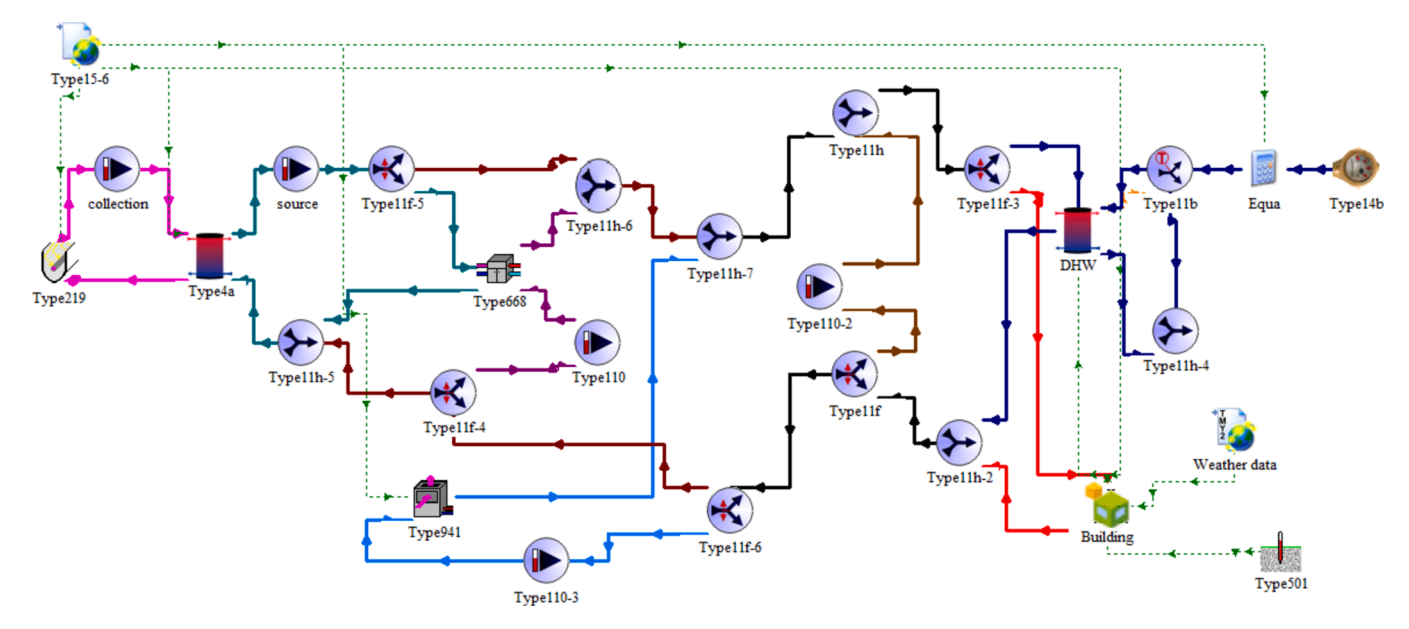


Fig. 3. TRNSYS model of the DSSAHP using CPC-CSC [21].

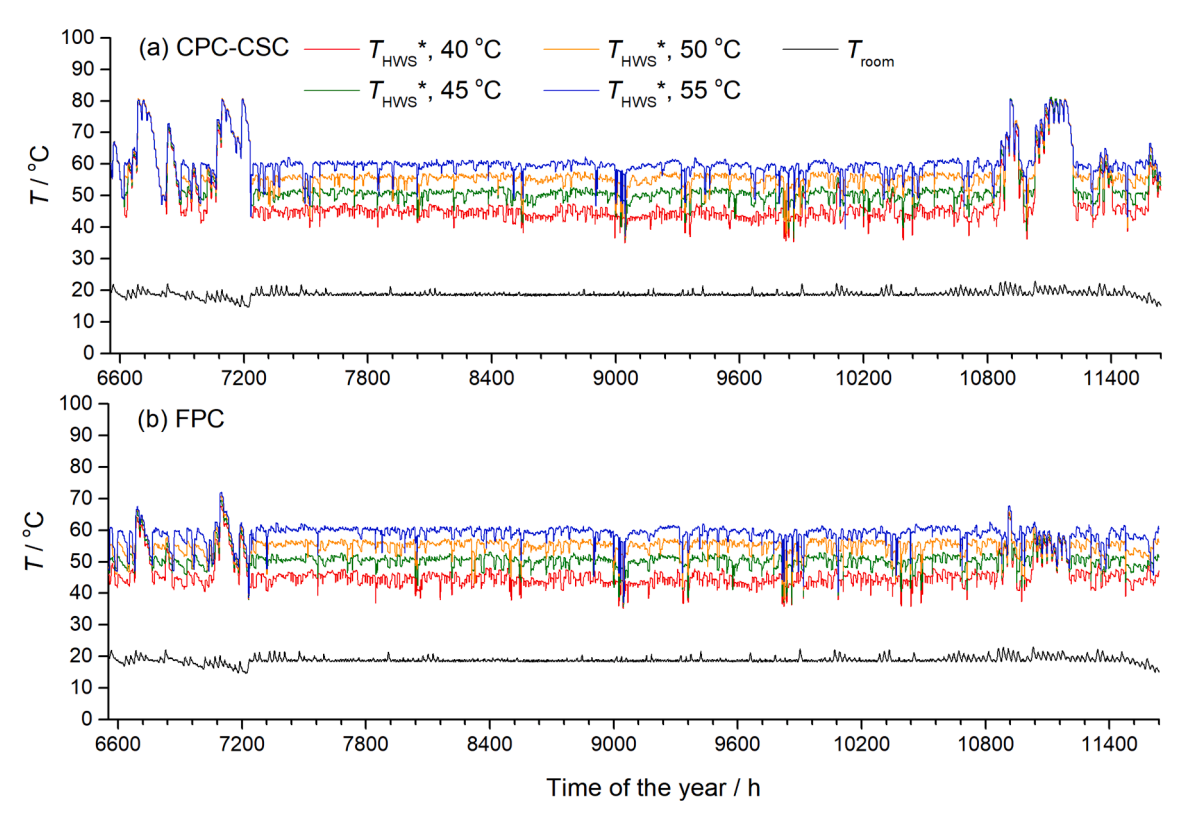


Fig. 4. Variations of indoor air temperature and hot water temperature at the outlet of TES tank 2 over a heating season for different T_{HWS}*.

test rig consists of CPC-CSC in the east–west direction, a hot water circulation loop and a data acquisition system. Two T-type thermocouples with an accuracy of \pm 0.1 K are inserted in the two mixers to measure the inlet and outlet bulk temperatures, respectively. 44 thermocouples are arranged at the inlet and outlet of each capillary tube. The turbine flow meter with an accuracy of 1 % measures the mass flow rate of water. The solar irradiation intensity is measured by TES1333R solar radiation recorder (with an accuracy of \pm 10 W/m²).

Two experiments were conducted to test the influence of solar irradiance ($290\,\text{W/m}^2$ to $1000\,\text{W/m}^2$) and inlet water temperature ($290\,\text{K}$ to

345 K). The experimental conditions are summarised in Table 1. The errors between the numerical and experimental results are $8.5\,\%$ and $15\,\%$ for case 1 and case 2, respectively. The good agreements between experimental and simulated results suggest the validity of the model.

2.2. Component module and system model in TRNSYS

The CPC-CSC module in TRNSYS is self-established based on the CFD simulation results from the model by ANSYS Fluent. The useful thermal energy absorbed by the capillary tube, Q_{SC} , is calculated by Eq. (1):

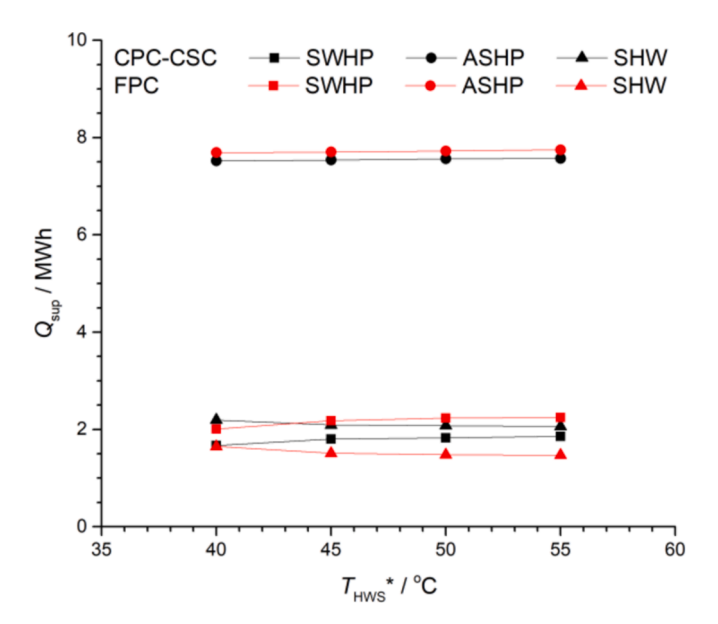


Fig. 5. Variations of heat for space heating and hot water by SWHP, ASHP and direct SHW against $T_{\rm HWS}^*$ for heating systems using CPC-CSC and FPC.

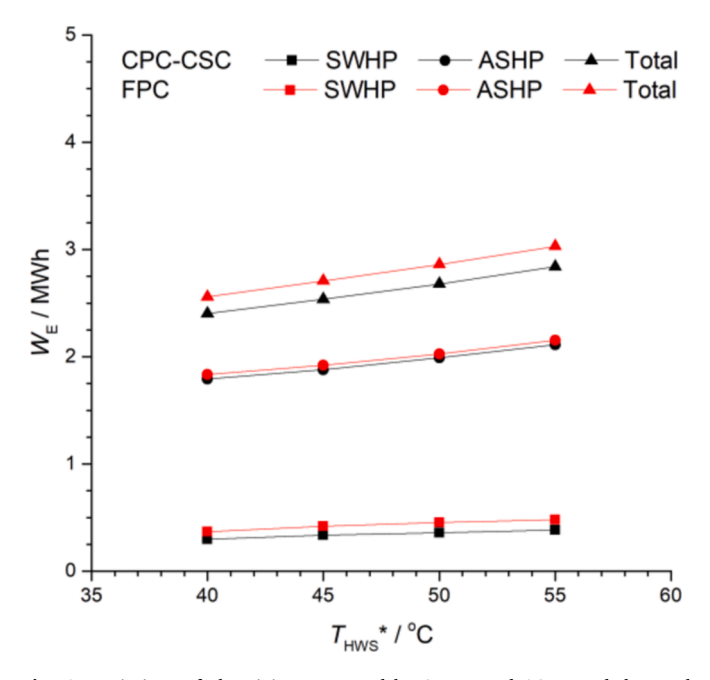


Fig. 6. Variations of electricity consumed by SWHP and ASHP and the total electricity consumed by the DSSAHP against $T_{\rm HWS}^*$ for DSSAHPs using CPC-CSC and FPC.

$$Q_{SC} = IA - Q_{loss,sc} = cm(T_{out} - T_{in})$$
(1)

where I is the solar irradiance for the tilted collector and A is the area of the CPC-CSC, m is the mass flow rate of water, c is the specific heat of water, $T_{\rm in}$ and $T_{\rm out}$ are the temperatures of water at the inlet and outlet of the collector. $Q_{\rm loss,sc}$ is the heat loss from the CPC-CSC. Dickes et al.'s [20] model is used to calculate the heat loss from the solar collector per meter (in length direction), $Q_{\rm loss}$:

$$\begin{split} Q_{loss} &= c_0 + c_1 (T_{sc} - T_{amb}) + c_2 (T_{sc} - T_{amb})^2 + c_3 T_{sc}^3 + I(c_4 \sqrt{\nu_a} \\ &+ c_5 T_{sc}^2) + \nu_a [c_6 + c_7 (T_{sc} - T_{amb})] + \sqrt{\nu_a} [c_8 + c_9 (T_{sc} - T_{amb})] \end{split} \tag{2}$$

where T_{sc} and T_{amb} are the collector temperature and ambient air

temperature, respectively, and v_a is wind velocity.

According to the operation parameters of the DSSAHP system, the water temperature at the inlet of the CPC-CSC varies from -5 °C to 80 °C. The operation performances of the CPC-CSC under the working conditions are numerically simulated by ANSYS Fluent, covering the weather conditions in the UK. In the CFD simulations, the water flow rate of the CPC-CSC is 7.23 kg/h-m².

The CFD simulation results are set to be training group and test group (3):1) to obtain the following empirical formula of the linear heat loss:

$$\begin{split} Q_{loss} &= 0.1458 (T_{sc} \\ &- T_{amb}) + 2.384310^{-4} (T_{sc} - T_{amb})^2 - 5.830310^{-6} T_{sc}^3 + I(0.0013 \sqrt{\nu_a} \\ &+ 8.130210^{-7} T_{sc}^2) + \nu_a [-0.088 + 5.237710^{-4} (T_{sc} \\ &- T_{amb})] + \sqrt{\nu_a} [0.422 - 0.0104 (T_{sc} - T_{amb})] \end{split}$$

The goodness of fit is 0.9903 and 0.9915 for the training and test groups. This means that the obtained empirical formula has good fitness to the origin data. The CPC-CSC module in TRNSYS is built based on Eqs. (1) and (3).

3. Dual-source solar assisted heat pump

A heating system based on DSSAHP using CPC-CSC is shown in Fig. 2 [21]. The DSSAHP has a solar collection loop, a thermal energy storage (TES) 1 to water-refrigerant-evaporator loop, an air source heat pump (ASHP) loop, a space heating loop, a TES1–TES2 loop, a refrigerant-water-condenser to TES2 loop and a solar water heat pump (SWHP) loop. At sufficient solar irradiation, solar energy is converted into thermal energy and stored in TES tank 1. When the water temperature in TES tank 1 is higher than that in TES tank 2, TES tank 1 provides direct solar hot water for domestic heating. When the water temperature in TES tank 2 is below $T_{\rm HWS}{}^*$, if the water temperature in TES tank 1 is between the ambient temperature and that in TES tank 2, SWHP works; if the temperature of water in TES tank 1 is lower than the ambient temperature, ASHP works.

3.1. Working conditions

The system is aimed to serve an SFH 45 building in London for space heating and hot water. The hot water consumption is assumed to be 300 L/day. The reference SFH 45 building is established following the instructions in [22]. The space hasting period is determined to be October 29th to April 24th in London to maintain indoor air temperature above 15 °C. For convenience, the heating season is set from 1st October to 30th April to compare the operation performance of the heating system. In the heating season, the designed indoor temperature is around 20 °C. This corresponds to the peak heating load of 3.53 kW and the average heating load of 1.76 kW in London.

To evaluate the operation performance of the system with different $T_{\rm HWS}^*$, $T_{\rm HWS}^*$ is set to be 40 °C, 45 °C, 50 °C and 55 °C. The highest limit for the water temperature in the TES tanks is set to be 80 °C for safety. Hot water temperature at the outlet of the water draw is set to be 40 °C to avoid scalding [23]. The water draws are set to be four 15-minute water draws of 300 L/h per day.

3.2. Numerical simulation model in TRNSYS

Operation performances of the DSSAHP system using CPC-CSC and FPC are simulated over a whole year. The numerical simulation starts in summer with a time step of 1 min. The CPC-CSC is modeled based on analyses in section 2 with a collector area of 8 m² and the FPC is set at the same collector area. In the TRNSYS model, a SWHP module and an ASHP module are used to represent the SWHP and ASHP modes of the dual-source HP unit with a heating capacity of 8 kW. The parameters for

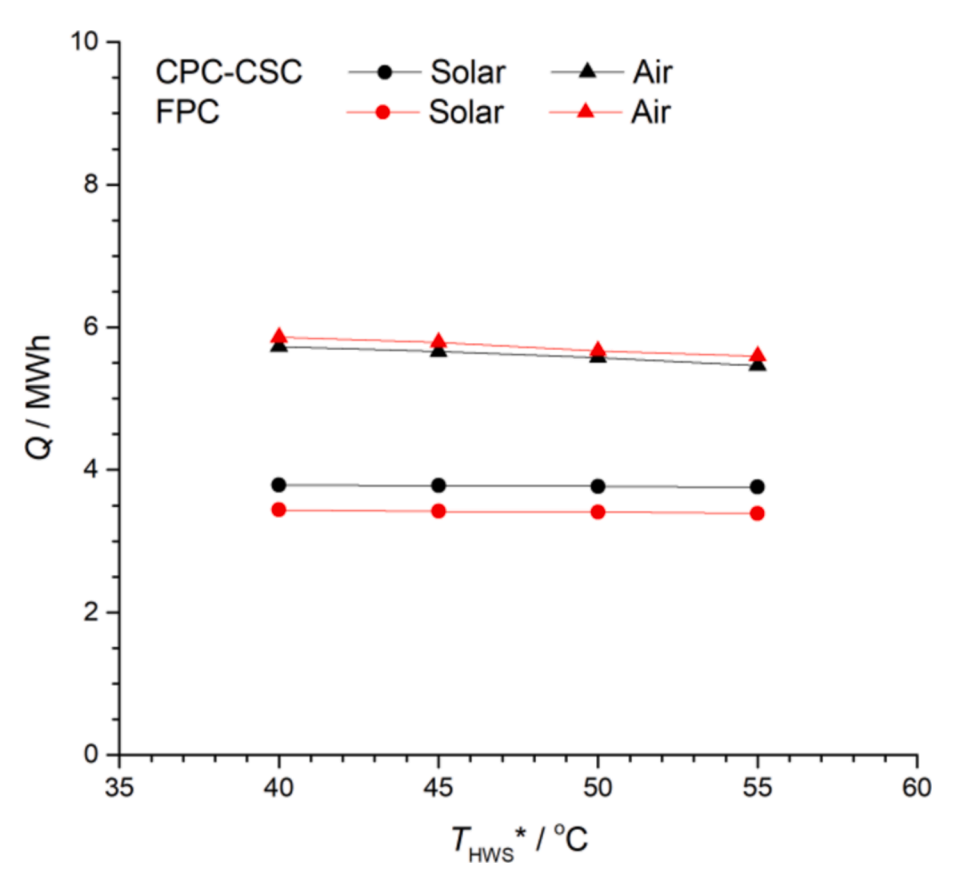


Fig. 7. Variation of thermal energy (Q) extracted from solar energy and ambient air against $T_{\rm HWS}^*$ for DSSAHPs using CPC-CSC and FPC.

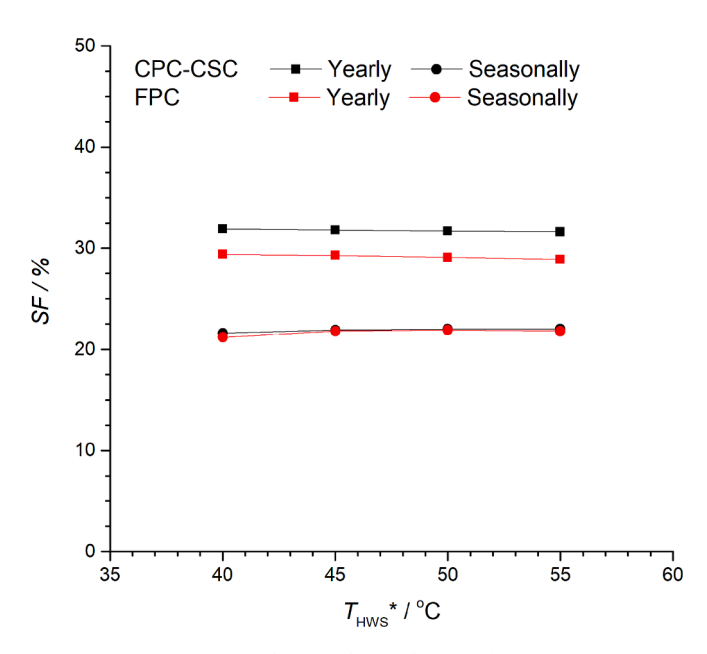


Fig. 8. Variations of year and seasonal SF with $T_{\rm HWS}^*$ for DSSAHPs using CPC-CSC and FPC.

the HP modules are user-defined according to the sample files of real HP units. Parameter selection for the modules and the schematic of the system model are displayed in Table 2 and Fig. 3 [21].

3.3. System performance

Operation performances of the DSSAHP system are mainly evaluated

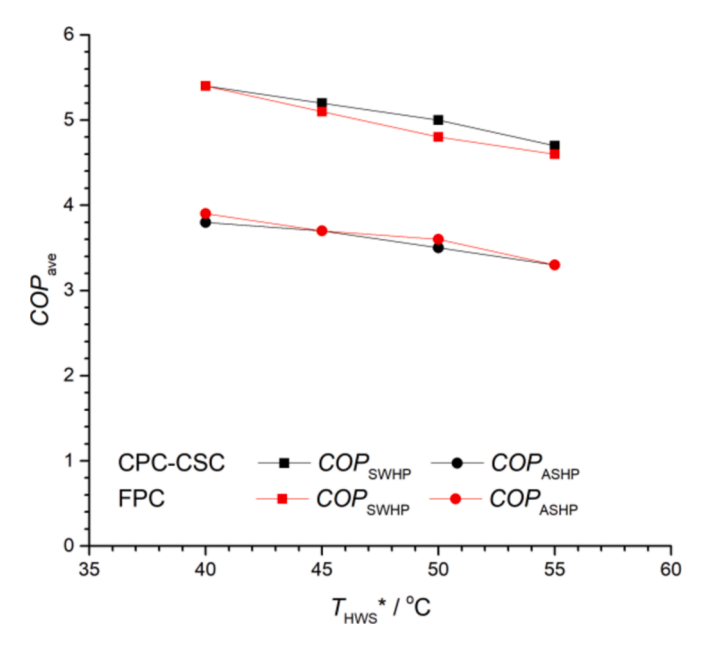
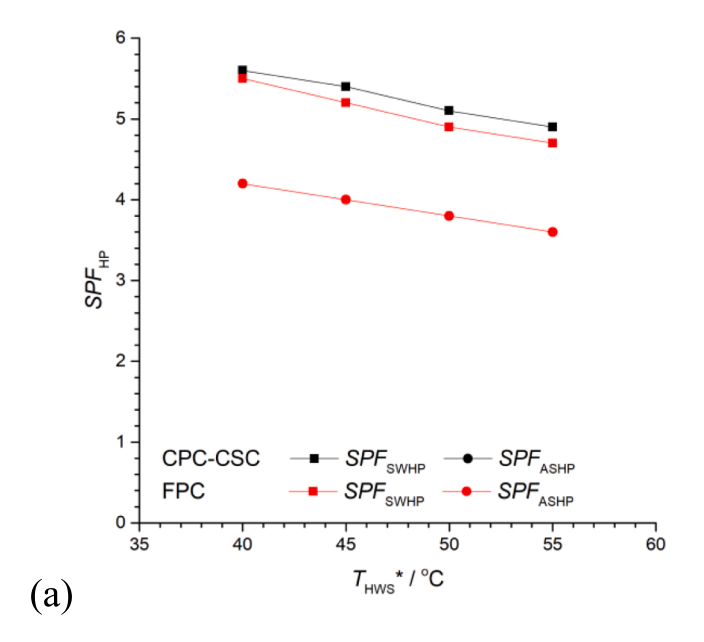


Fig. 9. Averaged *COP* of SWHP and ASHP with $T_{\rm HWS}^*$ for DSSAHPs using CPC-CSC and FPC.

by *COP*, solar fraction (*SF*) and *SPF*. *COP* represents the proportion of the heat provision from an HP unit, $Q_{\rm HP}$, to the corresponding amount of electricity consumed, $W_{\rm HP}$, given by Eq. (4):

$$COP = Q_{HP}/W_{HP} \tag{4}$$

SF represents the proportion of utilised solar energy to the total heat



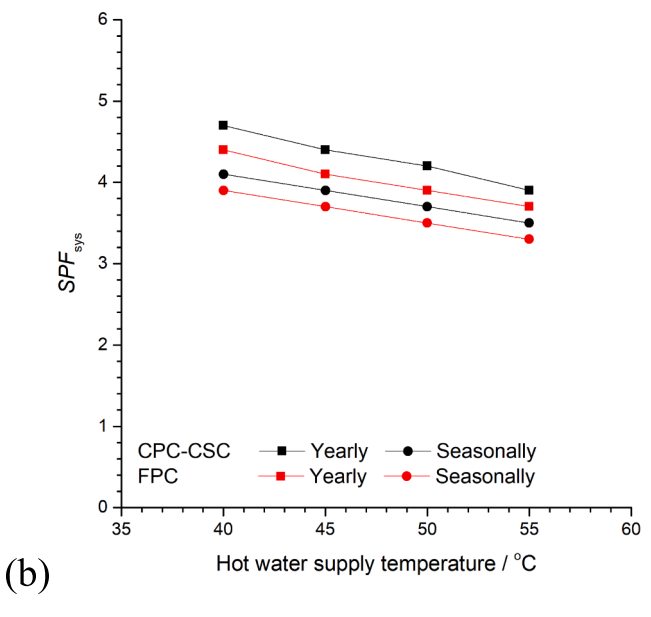


Fig. 10. Variations of year and seasonal SPF_{HP} and SPF_{sys} with T_{HWS}^* for DSSAHPs using CPC-CSC and FPC.

provision of the DSSAHP, given by Eq. (5):

$$SF = \frac{\int Q_{\text{su}} dt}{\int (Q_{\text{SH}} + Q_{\text{HW}}) dt}$$
 (5)

where Q_{su} is the utilised solar energy, Q_{SH} plus Q_{HW} is the total heat provision of the DSSAHP. *SPF* represents the proportion of heat provision to the amount of electricity consumed during a given period, given by Eq. (6):

$$SPF = \frac{\int Qdt}{\int Wdt} \tag{6}$$

where Q is the heat provision and W is the electricity consumed by the heating system or the HP accordingly.

4. Results and discussion

The heating performances of the DSSAHP using CPC-CSC and FPC with different $T_{\rm HWS}^*$ are investigated in TRNSYS 17. The daily operation performance for low temperature heating of DSSAHP using CPC-CSC is analysed in detail.

4.1. Comparison of low temperature heating operation performance

Fig. 4 shows the variations of indoor air temperature and hot water supply temperature for different designed T_{HWS}* during the heating season. It can be seen that in heating periods, at all T_{HWS}^* , both the DSSAHP can generally provide sufficient thermal energy and maintain the hot water temperature in TES tank 2 (T_{HWS}) around 5 °C above the $T_{\rm HWS}^*$. The variations of $T_{\rm HWS}$ have two main reasons: heat provision from the DSSAHP and heat supply to the load. When hot water is drawn for supply, cold mains water and cold water after space heating enters the TES tank 2 to compensate for the water draw. T_{HWS} varies in a larger range for higher T_{HWS}* due to the larger temperature difference. For higher T_{HWS}^* , since T_{HWS} varies in a larger range and is easier to drop below $T_{\rm HWS}^*$, more heat provision is required from the DSSAHP. The response to $T_{\rm HWS}$ drop of the DSSAHP using CPC-CSC is faster, especially for lower T_{HWS}*, showing benefits to the thermal comfort of low temperature heating. In non-heating periods, where direct solar hot water (SHW) works to provide thermal energy, DSSAHP using CPC-CSC can more often have higher T_{HWS} than a system using FPC.

Fig. 5 shows the variations of heat for space heating and hot water by SWHP, ASHP and direct SHW against T_{HWS}^* for heating systems using CPC-CSC and FPC over a year. Generally, for the system using CPC-CSC, the heat provision from ASHP and SWHP is less than that for the system using FPC, by around 2.2 % and 16.7 %; but that from direct SHW is obviously more than that from the system using FPC, by around 32.9 %. As T_{HWS}* decreases from 55 °C to 40 °C, for the system using CPC-CSC, the heat provision by SWHP and ASHP decreases from 1.86 MWh to 1.67 MWh and from 7.57 MWh to 7.52 MWh, respectively, and that for the system using FPC decreases from 2.25 MWh to 2.00 MWh and from 7.75 MWh to 7.69 MWh, respectively. At the same time, heat provision by direct SHW increases from 2.06 MWh to 2.19 MWh for DSSAHP using CPC-CSC and from 1.47 MWh to 1.65 MWh for DSSAHP using FPC. For DSSAHP using CPC-CSC, the decrease in $T_{\rm HWS}{}^*$ has more influence on the heat provision from SWHP (-10 %) and direct SHW (6.4 %) than on that from ASHP (-0.6 %).

Fig. 6 shows variations of electricity consumed by SWHP and ASHP and the total electricity consumed by the DSSAHP against $T_{\rm HWS}^*$ over a year. Overall, DSSAHP using CPC-CSC can reduce electricity consumption by 6.1 % compared with DSSAHP using FPC. Electricity savings from ASHP, SWHP and pumps are 2.1 %, 19.0 % and 13.5 %, respectively. As $T_{\rm HWS}^*$ decreases from 55 °C to 40 °C, for the system using CPC-CSC, electricity consumption by ASHP, SWHP and pumps decreases from 2.11 MWh to 1.79 MWh, from 0.38 MWh to 0.30 MWh and from 0.35 MWh to 0.31 MWh, respectively; those for DSSAHP using FPC decrease from 2.16 MWh to 1.83 MWh, from 0.48 MWh to 0.37 MWh and from 0.40 MWh to 0.36 MWh, respectively. For DSSAHP using CPC-CSC, the decrease in $T_{\rm HWS}^*$ apparently reduces the electricity consumption from ASHP (15.0 %), SWHP (22.2 %) and pumps (10.3 %).

Fig. 7 shows the variation of thermal energy (Q) extracted from solar energy and ambient air against $T_{\rm HWS}{}^*$ for DSSAHP over a year. Compared with DSSAHP using FPC, DSSAHP using CPC-CSC collects more thermal energy from solar energy (10.2%) and less thermal energy from ambient air (2.2%). As $T_{\rm HWS}{}^*$ decreases from 55 °C to 40 °C, for DSSAHP using CPC-CSC, thermal energy collections from solar energy and ambient air increase from 3.76 MWh to 3.79 MWh and from 5.46 MWh to 5.73 MWh; those for DSSAHP using FPC increase from 3.39 MWh to 3.44 MWh and from 5.59 MWh to 5.86 MWh. For DSSAHP using CPC-CSC, the decrease in $T_{\rm HWS}{}^*$ slightly increases thermal energy obtained from solar energy (0.8%) and ambient air (4.9%).

Energy & Buildings 324 (2024) 114903

Table 3Overall performance of the DSSAHPs using CPC-CSC and FPC operating in London.

System	Period		CPC-CSC					FPC				
•			40	45	50	55	40	45	50	55		
Heat provision (kWh)	HW	Heating-	2235.4	2237.6	2238.2	2237.8	2235.1	2237.8	2238.6	2238.2		
		Non-heating-	1427.1	1427.4	1427.5	1427.4	1427.4	1427.8	1428.3	1428.0		
	SH		7520.1	7526.7	7532.9	7525.0	7520.3	7519.7	7528.1	7522.9		
	Total		11182.6	11191.7	11198.6	11190.2	11182.7	11185.4	11195.0	11189.1		
Heat provision(kWh)	SWHP		1672.2	1802.6	1829.8	1859.4	2007.7	2180.5	2234.8	2248.2		
	ASHP		7522.7	7538.0	7564.9	7571.7	7692.0	7703.0	7723.4	7749.5		
	Solar	Heating-	734.8	675.5	676.0	675.0	424.8	366.9	355.7	360.2		
		Non– heating-	1459.8	1417.3	1401.5	1387.8	1226.8	1142.9	1123.8	1110.2		
Electricity consumption	SWHP		297.7	336.6	357.6	382.6	367.4	418.5	455.6	479.9		
(kWh)	ASHP		1794.1	1879.4	1989.3	2110.4	1832.5	1919.8	2024.5	2155.0		
	Water	Heating-	274.0	283.6	295.9	310.1	304.6	314.5	326.4	341.3		
	pumps	Non-heating-	36.4	36.0	35.9	35.8	54.4	53.5	53.1	53.2		
	Total	· ·	2402.2	2535.6	2678.8	2838.8	2558.9	2706.1	2859.6	3029.5		
SPF_{HP}	SWHP		5.6	5.4	5.1	4.9	5.5	5.2	4.9	4.7		
	ASHP		4.2	4.0	3.8	3.6	4.2	4.0	3.8	3.6		
COPave	SWHP		5.4	5.2	5.0	4.7	5.4	5.1	4.8	4.6		
	ASHP		3.8	3.7	3.5	3.3	3.9	3.7	3.6	3.3		
Solar thermal energy (kWh)	To SWHP		1374.5	1466.0	1472.2	1476.8	1640.2	1762.0	1779.2	1768.3		
	To end use	Heating-	734.8	675.5	676.0	675.0	424.8	366.9	355.7	360.2		
		Non-heating-	1459.8	1417.3	1401.5	1387.8	1226.8	1142.9	1123.8	1110.2		
	Total		3789.0	3777.1	3768.8	3757.8	3439.4	3419.5	3407.8	3387.4		
Thermal energy from ambient air (kWh)		5728.6	5658.6	5575.5	5461.3	5859.5	5789.2	5699.0	5594.5			
SF	Heating season		21.6 %	21.9 %	22.0 %	22.0 %	21.2 %	21.8 %	21.9 %	21.8 %		
	Yearly		31.9 %	31.8 %	31.7 %	31.6 %	29.4 %	29.3 %	29.1 %	28.9 %		
$SPF_{ m sys}$	Heating season		4.1	3.9	3.7	3.5	3.9	3.7	3.5	3.3		
	Yearly		4.7	4.4	4.2	3.9	4.4	4.1	3.9	3.7		

Note: Heating-: Heating season; Non-heating-: Non-heating season.

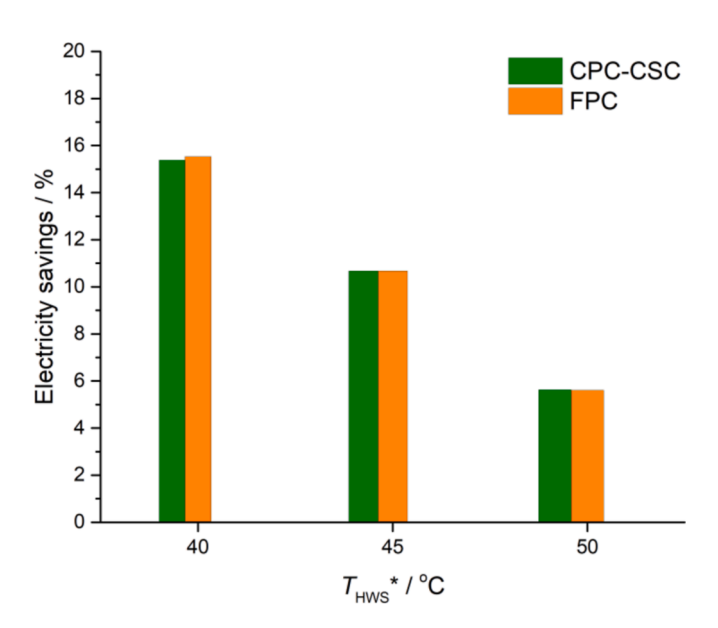


Fig. 11. Electricity savings at $T_{\rm HWS}^*$ of 40 °C, 45 °C and 50 °C compared with electricity consumption at $T_{\rm HWS}^*$ of 55 °C for DSSAHP using CPC-CSC and FPC.

Fig. 8 shows the variations of year and seasonal SF with $T_{\rm HWS}^*$ for DSSAHP over a year. The year SF of DSSAHP using CPC-CSC is around 8.5 % higher than that of DSSAHP using FPC while the seasonal SF values for DSSAHP using both CPC-CSC and FPC are generally the same. As $T_{\rm HWS}^*$ decreases from 55 °C to 40 °C, year SF values for systems using CPC-CSC and FPC slightly increase from 31.6 % to 31.9 % and from 28.9 % to 29.4 %. The seasonal SF values for systems using CPC-CSC and FPC slightly decrease from 22.0 % to 21.6 % and from 21.8 % to 21.2 %, respectively.

Fig. 9 shows the averaged COP of SWHP and ASHP with $T_{\rm HWS}^*$ for DSSAHP over a year. The difference between systems using CPC-CSC

and FPC is complex since using different solar collectors affects both the evaporating and condensing temperatures and thus the influence on heat pump operation performance is complex. As $T_{\rm HWS}^*$ decreases from 55 °C to 40 °C, for systems using CPC-CSC, $COP_{\rm ASHP}$ and $COP_{\rm SWHP}$ increase from 3.3 to 3.8 and from 4.7 to 5.4; those for the system using FPC increase from 3.3 to 3.9 and from 4.6 to 5.4. For the system using CPC-CSC, the decrease in $T_{\rm HWS}^*$ significantly increases $COP_{\rm ASHP}$ and $COP_{\rm SWHP}$ by 15.2 % and 14.9 %.

Fig. 10 shows the variations of year and seasonal SPF of ASHP (SPF_{ASHP}), SWHP (SPF_{SWHP}) and system (SPF_{sys}) with T_{HWS}^* over a year. DSSAHP using CPC-CSC shows higher SPF_{SWHP} than DSSAHP using FPC, by around 40 %; SPF_{ASHP} for both systems is almost the same. At the system level, DSSAHP using CPC-CSC has higher both seasonal (5.5 %) and year SPF_{sys} (7.0 %) compared with the system using FPC. As T_{HWS} * decreases from 55 $^{\circ}$ C to 40 $^{\circ}$ C, SPF_{SWHP} values for systems using CPC-CSC and FPC increase from 4.9 to 5.6 and from 4.7 to 5.5; SPF_{ASHP} for both systems increase from 3.6 to 4.2. At the same time, for the system using CPC-CSC, seasonal and year SPF_{sys} increase from 3.5 to 4.1 and from 3.9 to 4.7; those values for the system using FPC increase from 3.3 to 3.9 and from 3.7 to 4.4. For DSSAHP using CPC-CSC, the decrease in $T_{HWS}{}^{\star}$ significantly increases \textit{SPF}_{ASHP} and \textit{SPF}_{SWHP} by 16.7 % and 14.3 %, as well as seasonal and year $SPF_{\rm sys}$, by 17.1 % and 20.5 %. The details for the operation performance of the heating systems using CPC-CSC and FPC with different T_{HWS}^* are given in Table 3

Fig. 11 shows the yearly electricity savings at $T_{\rm HWS}^*$ of 40 °C, 45 °C and 50 °C compared with electricity consumption at $T_{\rm HWS}^*$ of 55 °C. Systems using both CPC-CSC and FPC have similar electricity saving rate at different $T_{\rm HWS}^*$ under the weather conditions in London. As $T_{\rm HWS}^*$ decreases from 55 °C to 50, 45 and 40 °C, electricity consumption is saved by 5.6 %, 10.7 % and 15.4 %.

4.2. Low temperature heating operation performance on the coldest day

Fig. 12 shows the daily variations of thermal energy charged and discharged in the TES tank 2 for different T_{HWS}^* . For different T_{HWS}^* , the daily variations on thermal energy storage show a similar trend though

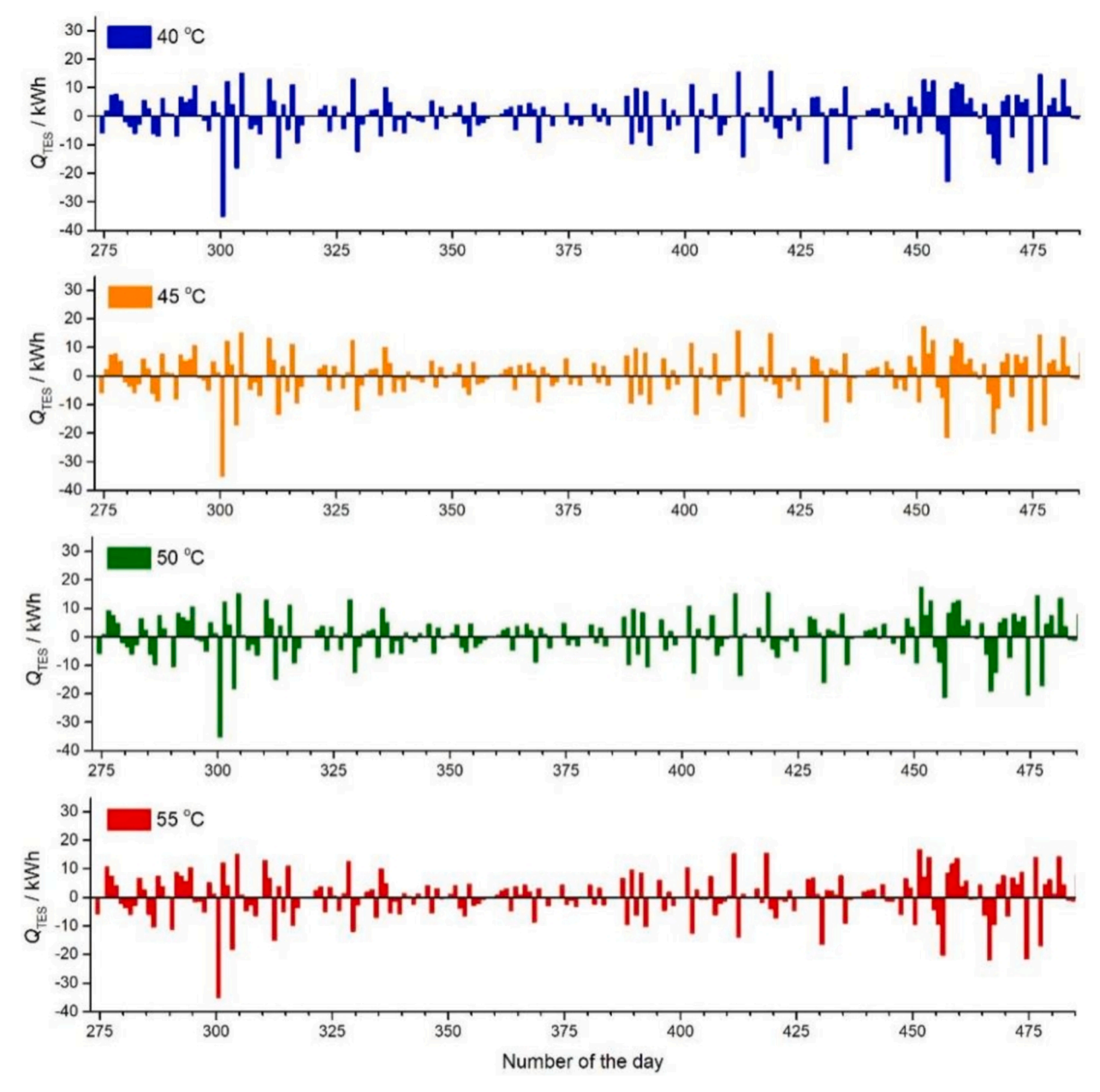


Fig. 12. Daily variations of Q_{TES} charged (positive) and discharged (negative) over a heating season for different T_{HWS}^* .

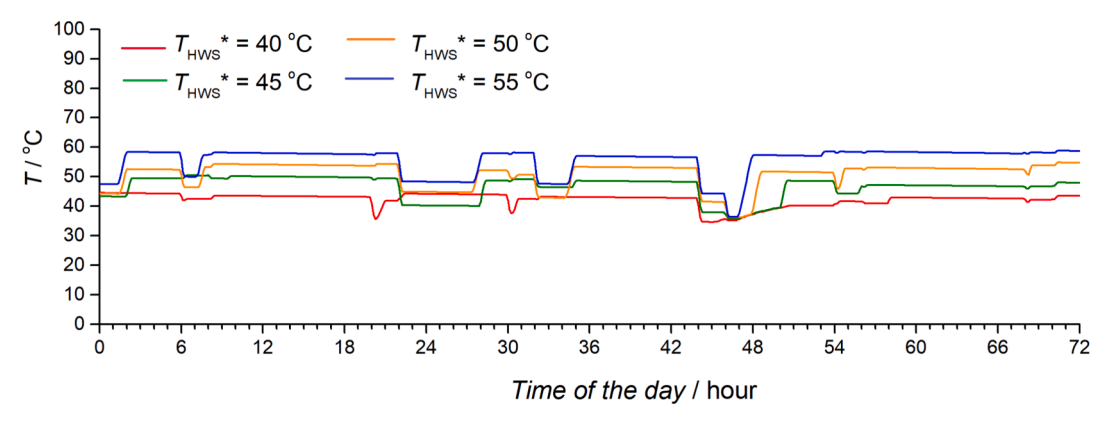


Fig. 13. Variations of hot water temperature at the outlet of TES tank 2 on the 11-13th day for different $T_{\rm HWS}^*$.

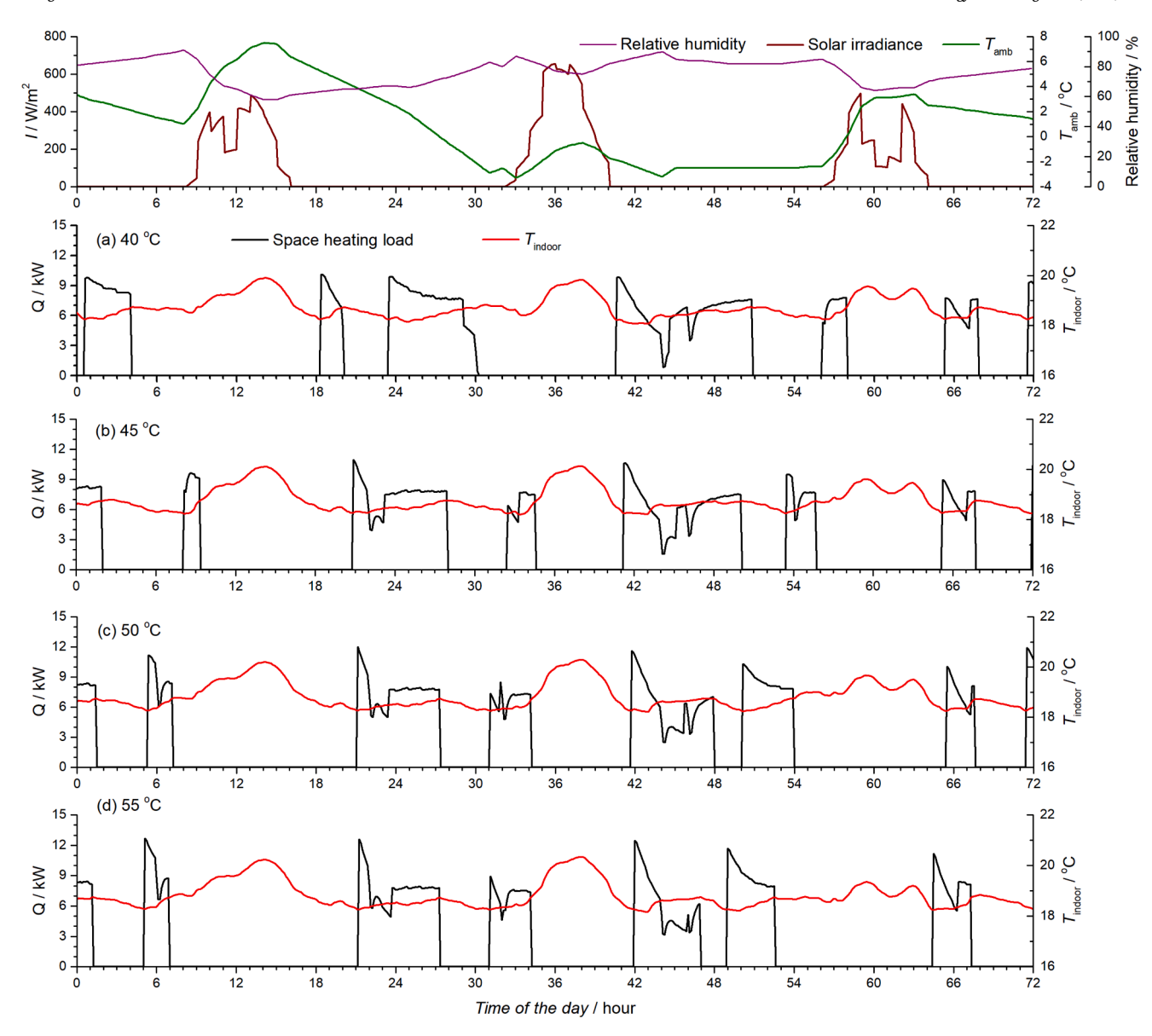


Fig. 14. Variations of space heating load and indoor air temperature on the 11-13th day for different T_{HWS}*.

 $T_{\rm HWS}^*$ affects the storage capacity in TES tank 2. However, for the heating system at the same $T_{\rm HWS}^*$ but different collector area of CPC-CSC, the thermal energy in TES tank 2 ($Q_{\rm TES}$) charged and discharged varies more apparently [21]. This suggests that the collector, rather than the $T_{\rm HWS}^*$, has more influence on the TES performance of the DSSAHP. Thus, to modify the operation performance of low temperature heating, optimisation in solar collector can be a useful approach.

Operation performance for low temperature heating of the system using CPC-CSC on the 11-13th day (including the day where the lowest ambient air temperature occurs, the 12th day) is selected for the case study. Fig. 13 shows the variations of hot water temperature at the outlet of TES tank 2 for different $T_{\rm HWS}^*$. In most time, $T_{\rm HWS}$ are around 3 °C higher than $T_{\rm HWS}^*$ for all $T_{\rm HWS}^*$. The hot water supply is set at 6.00 am, 8.00 am, 8.00 pm and 10.00 pm. At that time, water in TES tank 2 transfers heat with mains water and its temperature would drop. It is seen that the minimum variation of actual heating temperature ($T_{\rm HWS}$) occurs at $T_{\rm HWS}^*$ of 40 °C, followed by $T_{\rm HWS}^*$ of 45 °C.

Fig. 14 shows the variations of space heating load and indoor air temperature for different $T_{\rm HWS}^*$. Due to the different temperature differences between $T_{\rm HWS}$ and indoor temperature, space heating load shows different characteristics for different $T_{\rm HWS}^*$. As $T_{\rm HWS}^*$ increases,

higher temperature difference brings higher heat transfer efficiency. As $T_{\rm HWS}^*$ increases from 40 to 45, 50 and 55 °C, the peak SH load increases from 10.11 kW to 10.95, 12.00 and 12.67 kW. The heat transfer rate is increased and thus the SH period is reduced. The SH periods are 27.13, 26.38, 25.75 and 24 h for $T_{\rm HWS}^*$ of 40, 45, 50 and 55 °C.

Fig. 15 shows the variations of heating supplied by ASHP and SWHP for different $T_{\rm HWS}^*$. On the 11-13th day, direct SHW cannot provide thermal energy to the end use. When both ASHP and SWHP do not operate, it refers to the periods that no thermal energy is required by end-use or by TES tank 2 to maintain the $T_{\rm HWS}^*$. For reference, water temperature in TES tank 1 ($T_{\rm TESI}$) and TES tank 2 ($T_{\rm HWS}$) are added. Though higher $T_{\rm HWS}^*$ brings less period of heating demand for end use, it increases the requirement for TES tank 2. Overall, for $T_{\rm HWS}^*$ of 40, 45, 50 and 55 °C, the operation periods of ASHP are 21.88, 21.5, 22.25 and 22 h; those of SWHP are 9.88, 10.13, 10.25 and 9.75 h; the heating periods for TES tank 2 solely are 4.62, 5.00, 6.75 and 7.75 h. On these days, the total heating provision is 1.84, 1.82, 1.87 and 1.84 MWh for $T_{\rm HWS}^*$ of 40, 45, 50 and 55 °C, where 23.60 %, 23.95 %, 23.44 % and 23.44 % is provided by SWHP and 76.40 %, 76.05 %, 76.56 % and 76.56 % is provided by ASHP.

Fig. 16 shows the variations of electricity consumed rate of ASHP,

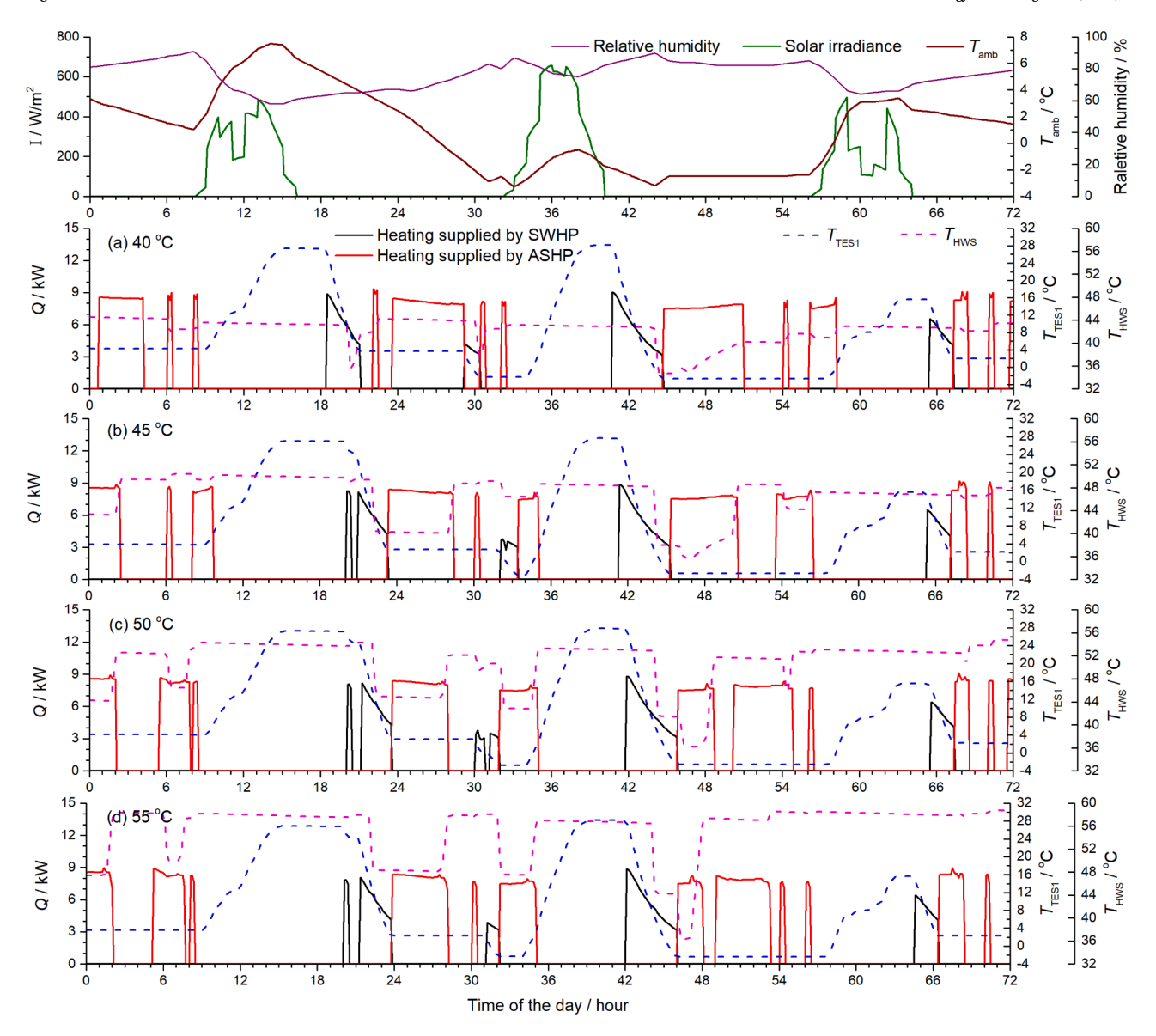


Fig. 15. Variations of heating supplied by ASHP and SWHP on the 11-13th day for different $T_{\rm HWS}^{\star}$.

SWHP and pumps for different T_{HWS}^* . Though heating power of ASHP is generally the same, for example, from 24.00 to 28.00 h, the electricity consume rate of ASHP increases as condensing temperature increases. This situation does not occur for SWHP in both systems since SWHP mainly works for the primary periods of heating where the condensing temperature is not apparently increased. According to the solar irradiance, SWHP mainly works after solar collection for a day. Then as stored water temperature in the TES tank 1 decreases below ambient temperature, ASHP works. At early morning where ambient temperature drops below store water temperature in TES tank 1, SWHP also works for a while, such as at around 30.00 h. For $T_{\rm HWS}^*$ of 40, 45, 50 and 55 °C, the average electricity consumption rates of ASHP are 2.16, 2.22, 2.31 and 2.42 kW; those of SWHP are 1.12, 1.13, 1.16 and 1.16 kW. Therefore, even though system at lower T_{HWS}^* may require longer operation periods, the total electricity consumption is reduced due to the lower average electricity consumption rate. On these days, the total electricity consumption is 520.19, 528.21, 564.58 and 576.13 kWh for T_{HWS}^* of 40, 45, 50 and 55 °C, where 16.73 %, 17.10 %, 16.66 % and 15.68 % is consumed by SWHP; 72.24 %, 71.94 %, 72.46 % and 73.45 % is consumed by ASHP; 11.02 %, 10.96 %, 10.88 % and 10.87 % is consumed by pumps.

Fig. 17 shows the variations of *COP* of ASHP (COP_{ASHP}), SWHP (COP_{SWHP}) and system (COP_{sys}) for different T_{HWS}^* . COP_{SWHP} is mainly in the range of 2.0–7.0 and the COP_{ASHP} is mainly in the range of 2.0–4.0. As T_{HWS}^* increases, COP_{SWHP} increases while COP_{ASHP} decreases. The variation trend of COP_{SWHP} is caused by the TES capacity in TES tank 2. Heat provision is urgently needed for DSSASHP at lower T_{HWS}^* , as shown in around 40th - 42nd hour. In the coldest days, solar irradiance is insufficient to compensate the usage of TES in TES tank 1. When the DSSAHP for higher T_{HWS}^* operates, its evaporating temperature is higher and the operation performance can be better. The COP_{ASHP} shows a common trend that, since the ambient temperature is generally the same, higher condensing temperature brings low system efficiency. It is interesting to find that, the COP_{SyS} can be in the range of 1.0–9.0, broader than the ranges of COP_{SWHP} and COP_{ASHP} . This is due to the time glide of demand and supply caused by TES in TES tank 2.

4.3. Low temperature heating performance on the day with direct solar hot water heating

Operation performance for low temperature heating of system using CPC-CSC on the 64-66th day is selected for case study where direct SHW

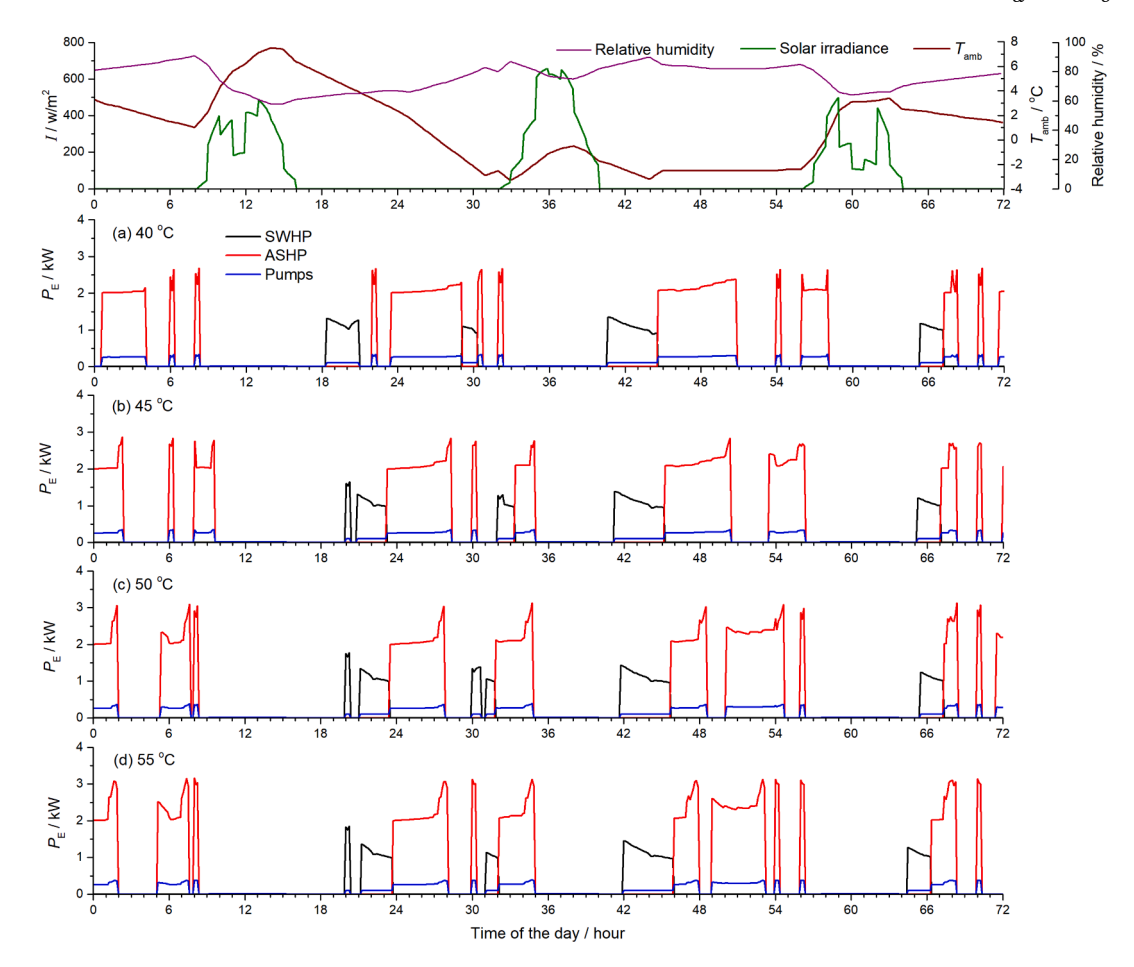


Fig. 16. Variations of electricity consumed rate of ASHP, SWHP and pumps on the 11-13th day for different T_{HWS}^* .

can provide heating. Fig. 18 shows the variations of hot water temperature at the outlet of TES tank 2 for different $T_{\rm HWS}^*$. In most time, $T_{\rm HWS}$ are around 5 °C higher than $T_{\rm HWS}^*$ for all $T_{\rm HWS}^*$. System using CPC-CSC has frequent variations in $T_{\rm HWS}$ because it uses more thermal energy stored in TES tank 1 via direct SHW and stored thermal energy left for SWHP is insufficient. Therefore, the system cannot respond quickly to increase the $T_{\rm HWS}$ when SWHP operates.

Fig. 19 shows the variations of space heating load and indoor air temperature for different $T_{\rm HWS}^*$. The SH periods are 13.00, 12.25, 11.88 and 11.25 h for $T_{\rm HWS}^*$ of 40, 45, 50 and 55 °C. As $T_{\rm HWS}^*$ increases from 40 to 45, 50 and 55 °C, the peak SH load increases from 11.95 kW to 14.50, 15.88 and 17.16 kW.

Fig. 20 shows the variations of heating supplied by ASHP, SWHP and direct SHW for different T_{HWS}^* . For reference, water temperature in TES tank 1 and TES tank 2 are added. Direct SHW can provide thermal energy to the end use among all three days in some cases. However, in some cases, though stored solar energy is sufficient to be used, the $T_{\rm HWS}$ is maintained higher than $T_{\rm HWS}^*$ and the operation of direct SHW is reduced. Thus, heat provision by direct SHW only contributes to a small portion of total heat provision. For $T_{\rm HWS}^*$ of 40, 45, 50 and 55 °C, for system using CPC-CSC, the operation periods of ASHP are 8.00, 7.88, 8.0 and 7.5 h; those of SWHP are 7.75, 8.0, 7.75 and 7.88 h; the heating periods for TES tank 2 solely are 2.75, 3.63, 3.87 and 4.13 h. On these days, for system using CPC-CSC, the total heating provision is 1.13, 1.12, 1.09 and 1.07 MWh for $T_{\rm HWS}^*$ of 40, 45, 50 and 55 °C, where 38.8 %, $40.0\,\%,\,40.1\,\%$ and $38.9\,\%$ is provided by SWHP; $48.8\,\%,\,48.2\,\%,\,50.5\,\%$ and 47.3 % is provided by ASHP; 12.5 %, 11.8 %, 9.4 % and 13.8 % is provided by direct SHW.

Fig. 21 shows the variations in electricity consumed rate of ASHP, SWHP and pumps for different $T_{\rm HWS}^*$. For $T_{\rm HWS}^*$ of 40, 45, 50 and 55 °C,

the average electricity consumption rates of ASHP are 2.16, 2.22, 2.37 and 2.44 kW; those of SWHP are 1.19, 1.25, 1.26 and 1.29 kW. On these days, for the system using CPC-CSC, the total electricity consumption is 240.60, 248.28, 259.18 and 256.14 kWh for $T_{\rm HWS}{}^*$ of 40, 45, 50 and 55 °C, where 30.7 %, 32.2 %, 30.2 % and 31.6 % is consumed by SWHP; 57.5 %, 56.4 %, 58.6 % and 57.2 % is consumed by ASHP; 11.8 %, 11.4 %, 11.2 % and 11.2 % is consumed by pumps.

Fig. 22 shows the variations of *COP* of ASHP, SWHP and system for different $T_{\rm HWS}^*$. These on the 64-66th days are apparently different from those on 11-13th days. $COP_{\rm SWHP}$ is mainly in the range of 2.0–8.0 and the $COP_{\rm ASHP}$ is mainly in the range of 2.0–4.0. Both $COP_{\rm SWHP}$ and $COP_{\rm ASHP}$ increase as $T_{\rm HWS}^*$ decreases. The $COP_{\rm Sys}$ is mainly in the range of 3.0–9.0.

5. Environmental and economic analyses

5.1. Life-span environmental analysis

For the DSSAHP system, total equivalent warming impact (*TEWI*) is used to describe both direct and indirect impacts on CO₂ emission caused by direct refrigerant loss and the electricity consumption and the corresponding generation, defined as Eq. (7) [24]:

$$TEWI = (GWP \times L \times n) + [GWP \times m \times (1 - a_{recovery})] + (n \times W_E \times \beta)$$
(7)

where *GWP* is the global warming potential of the refrigerant, 1430 for R134a; L is the refrigerant leakage rate per year (kg), 10 % of total refrigerant charge; n is the life span, 15 years; m is the refrigerant charge, 1.3 kg; α_{recovery} is the recycling factor of refrigerant, 0.7; W_E is the yearly

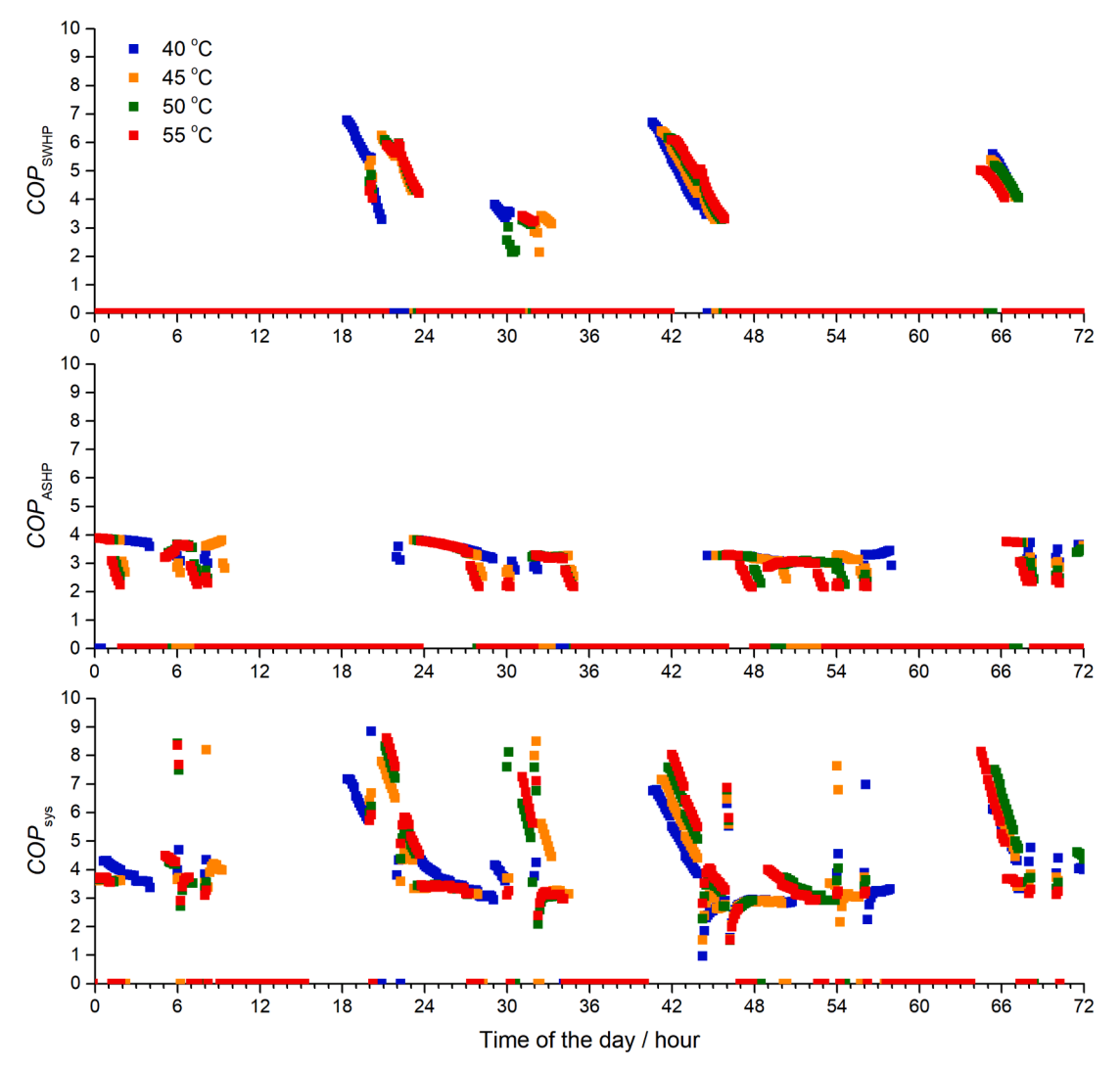


Fig. 17. Variations of COP of ASHP, SWHP and system on the 11-13th day for different $T_{\rm HWS}^*$.

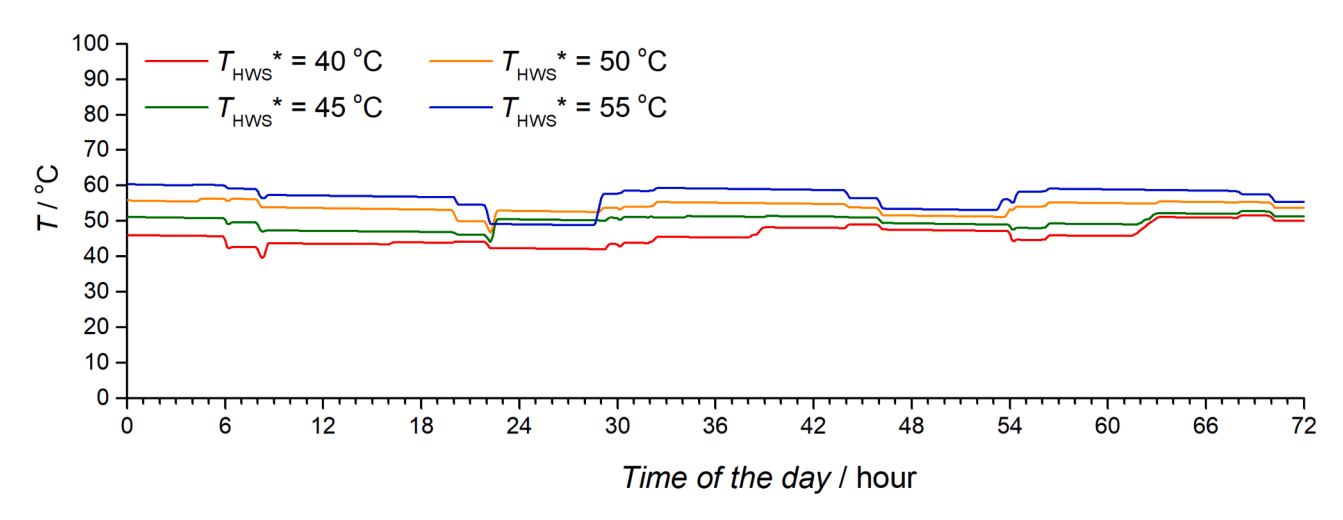


Fig. 18. Variations of hot water temperature at the outlet of TES tank 2 on the 64-66th day for different $T_{\rm HWS}^{\star}$.

electricity consumption; and β is the CO_2 emission ratio for electricity generation. In the UK, according to the Intergovernmental Panel on Climate Change, the CO_2 emission ratio for the electricity generation sector is calculated to be 0.254 kg/kWh [25].

For comparison, CO2 emissions of heating systems using fossil fuel

boilers are calculated with the same life span. According to [26], the ratios of CO_2 emission to heat provision of coal, oil, liquefied petroleum gas and natural gas are 0.517, 0.335, 0.262 and 0.267 kg/kWh. According to the yearly electricity consumption and heat provision in Table 3, the life-span CO_2 emission of DSSAHP and the equivalent fossil

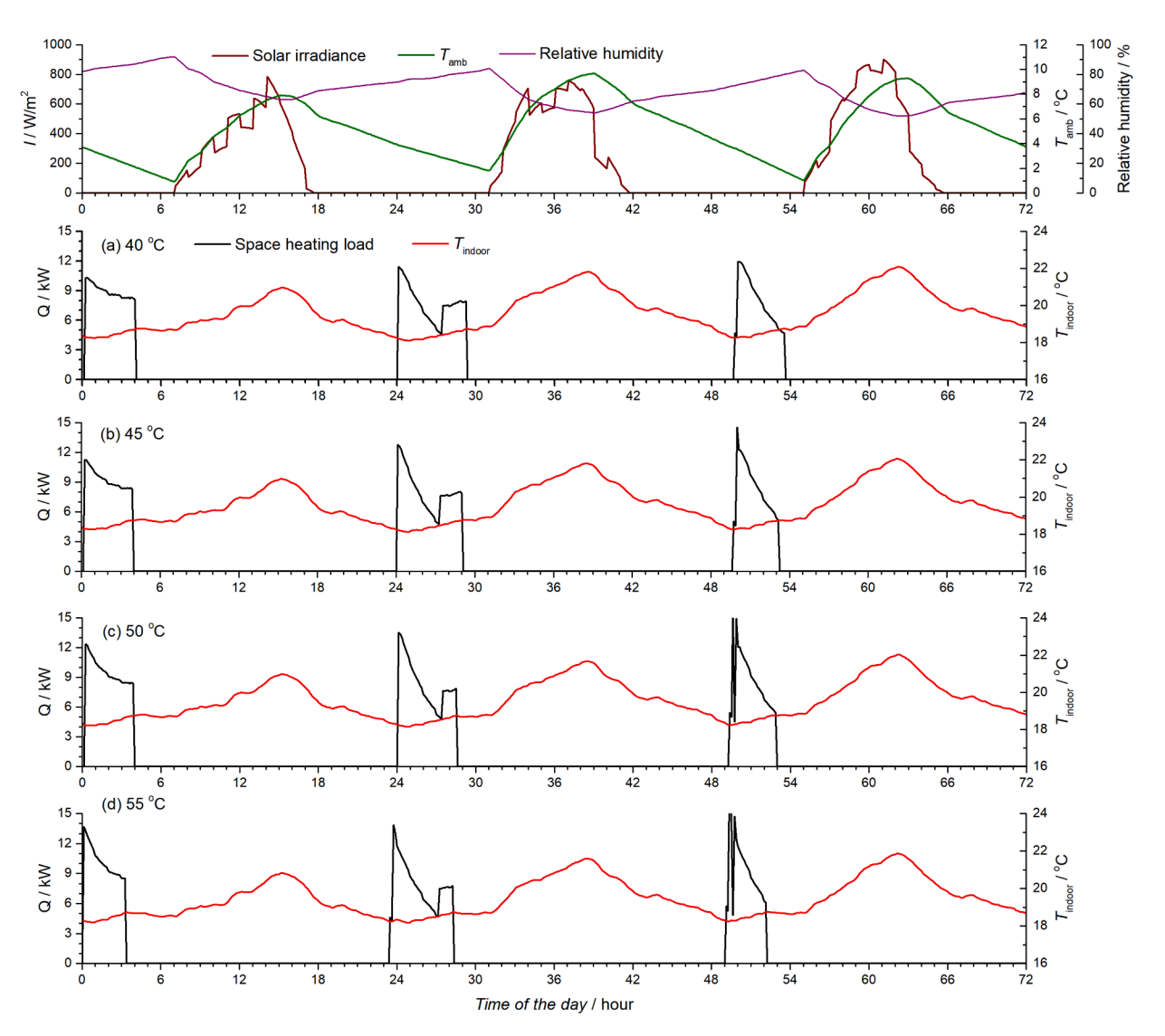


Fig. 19. Variations of space heating load and indoor air temperature on the 64-66th day for different $T_{\rm HWS}^{\star}$.

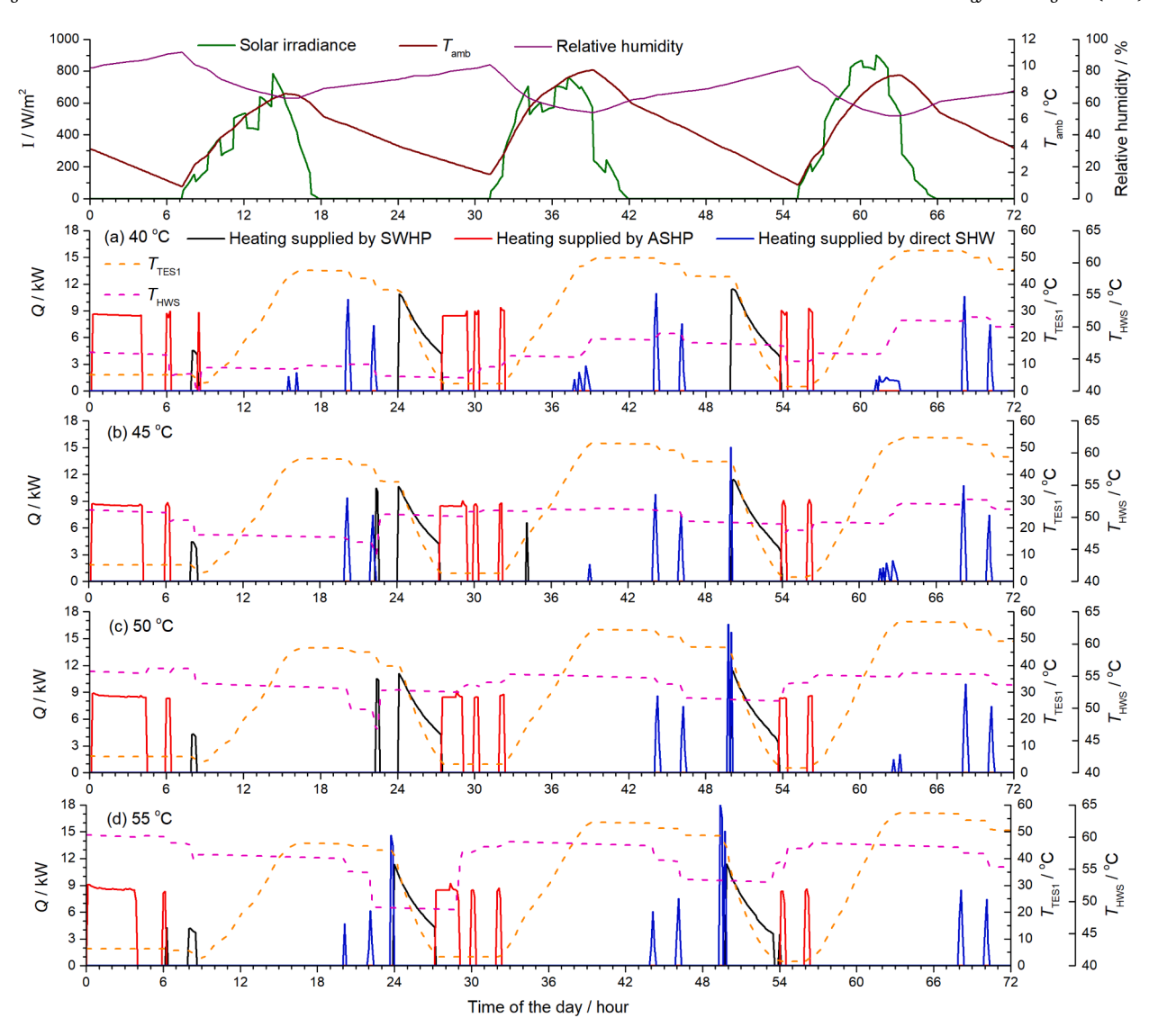


Fig. 20. Variations of heating supplied by ASHP, SWHP and direct SHW on the 64-66th day for different T_{HWS}*.

fuel heating systems are listed in Table 4.

It can be seen that, using DSSAHP can significantly reduce $\rm CO_2$ emission compare with using fossil fuel heating system. Generally, the TEWI of DSSAHP using R134a is only around 14.4 %, 22.2 %, 28.4 % and 27.9 % of $\rm CO_2$ emissions of heating system using coal, oil, liquefied petroleum gas and natural gas. With the development of eco-friendly refrigerants, further reduction in $\rm CO_2$ emission can be achieved from the direct impact of DSSAHP.

Using ultra-low temperature heating can decrease TEWI by 11.7 % and 12.0 % for DSSAHP using CPC-CSC and FPC. Compared with DSSAHP using FPC, DSSAHP using CPC-CSC has a reduction of around 4.6 % in TEWI. This illustrates a green potential for HP optimisation via using well-designed components and operation modes.

5.2. Economic analysis

Economic analyses of the DSSAHP heating system using CPC-CSC and FPC for low temperature heating are performed according to the electricity price in the UK. An electric heater is used as the benchmark for comparison. $W_{\rm tot}$ is the total electricity consumption of the heating systems, given by Eq. (8):

$$W_{tot} = (Q_{SH} + Q_{HW})/\eta \tag{8}$$

where η is the efficiency of electric heater.

 $P_{\rm pb}$ is the payback period of the heating systems against the electric heater, calculated by Eq. (9):

$$P_{pb} = C_i / C_{spy} \tag{9}$$

where C_i is the difference of the initial cost and C_{spy} is the cost saving per year, obtained by Eqs. (10) and (11).

$$C_i = C_{i0} - C_{ieh} \tag{10}$$

$$C_{spy} = C_{o0} - C_{oeh} \tag{11}$$

where C_{i0} and C_{ieh} are the initial costs of the heating system and the electric heater, C_{o0} and C_{oeh} are the operation costs of the heating system and the electric heater.

The efficiency of the electric heater is 0.95 [27]. The heat provision of the electric heater is set to be the average heat provision of the DSSAHP heating system, 11.19 MWh. The electricity price is obtained from statistics to be £72.34 per MWh (price in May 2024) [28]. Currently, the price of CPC collector is around twice of that of ETC [18]. Since CPC-CSC is a new collector in research and development status, price of ETC is adopted to assume CPC-CSC price after commercialisation. The prices of electric heater of 8 kW (£3000) [29], TES tank of 300

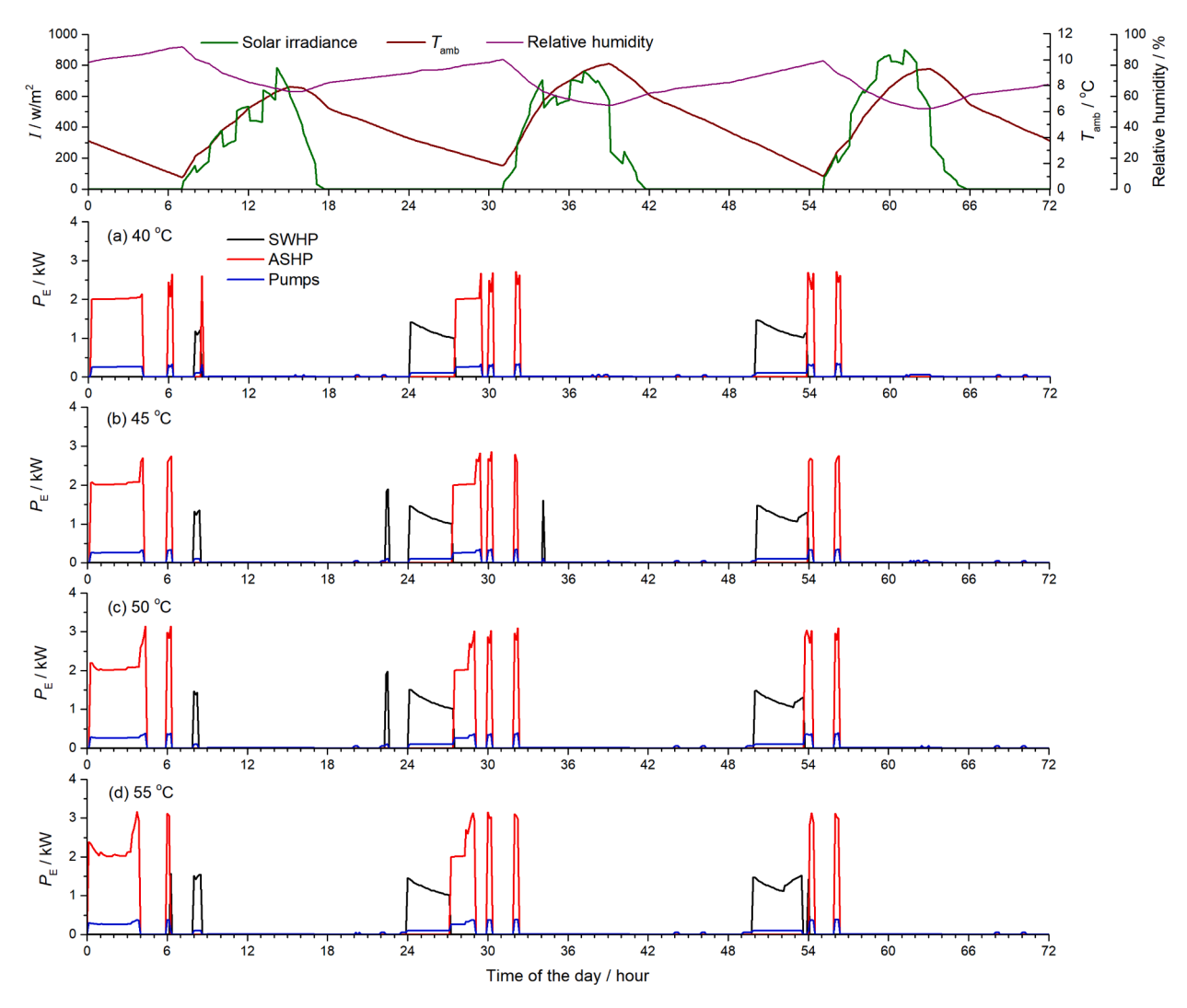


Fig. 21. Variations of electricity consumed rate of ASHP, SWHP and pumps on the 64-66th day for different $T_{\rm HWS}^*$.

L (£815) and 500 L (£1650) [30], water pump with a head of 10 m (£360) [31], flat plate collector [32] and evacuated tube collector [33] are obtained from UK domestic and European sellers. The price of heat pump is assumed based on UK government report [34]. Installation for for DSSAHP is assumed to be 6 h. The engineer fee is taken to be £80 per hour [35]. The economic analysis for DSSAHP heating system integrating CPC-CSC and FPC for low temperature heating is displayed in Table 5.

According to the economic analysis, it can be seen that the initial cost of the DSSAHP system using CPC-CSC is slightly higher than that of the system using FPC, by around 12.9 %. The operation cost per year of the DSSAHP system using CPC-CSC is reduced by 6.8 % compared with that of the system using FPC. Under the current electricity price, DSSAHP systems using CPC-CSC and FPC share a similar payback period of 11 \sim 12 years for different set heating temperatures. However, in 2022, electricity price arrived around £400 per MWh dramatically. In that case, the payback period can be reduced to around 2 years for both systems. The DSSAHP system using CPC-CSC shows comparable economic performance to that using FPC, with a mere extend in a payback period of around 1.9 %. Considering thermal comfort and environmental benefits, CPC-CSC can be acceptable for wide application to improve low temperature heating performance.

6. Conclusions

This paper investigates the ultra-low temperature heating performances of a DSSAHP heating system using CPC-CSC. The advantages of the system providing heating for the SFH 45 building in London have been analysed. The conclusions can be drawn below:

- Using CPC-CSC benefits the response speed of DSSAHP as low T_{HWS}*, improving the thermal comfort performance of ultra-low temperature heating. The collector, rather than the T_{HWS}*, has more influence on the TES performance of the DSSAHP. To further develop ultra-low temperature heating, innovation in solar collectors plays an important role.
- 2. Low temperature heating increases the application of renewable energies. For DSSSAHP using CPC-CSC, ultra-low temperature heating increases thermal energy obtained from solar energy (0.8 %) and ambient air (4.9 %).
- 3. Low temperature heating contributes to passive heating. For DSSAHP using CPC-CSC, low temperature heating has more influence on the heat provision from SWHP (-10~%) and direct SHW (6.4 %) than on that from ASHP (-0.6~%).
- 4. Compared with DSSAHP using FPC, the heating system using CPC-CSC can reduce *TEWI* by 4.6 % with a slight extension in payback period by 1.9 %.

L.W. Yang et al.

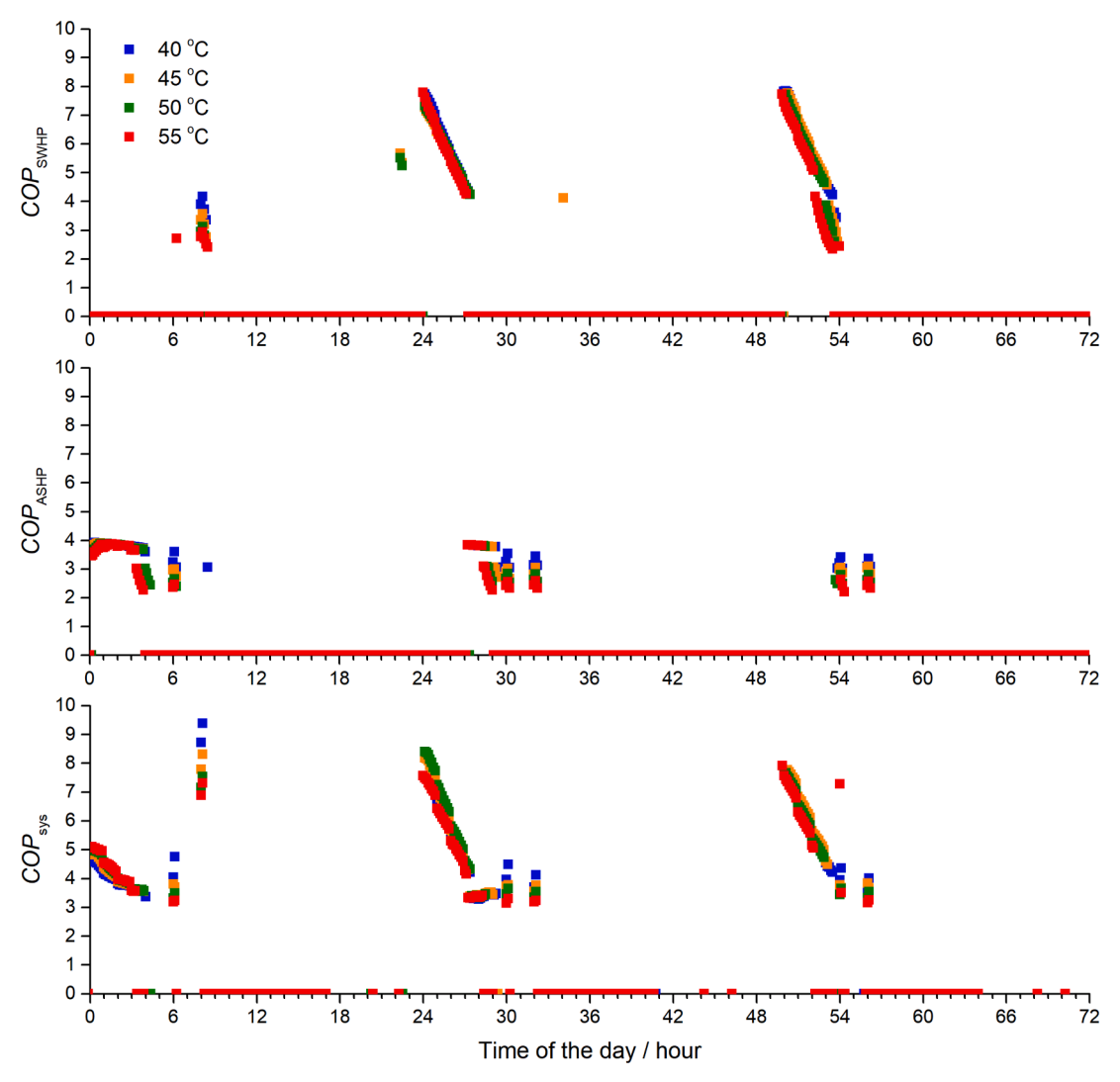


Fig. 22. Variations of COP of ASHP, SWHP and system on the 64-66th day for different $T_{\rm HWS}^*$.

Table 4 Life-span CO_2 emission of DSSAHP and equivalent fossil fuel heat systems (ton).

		CPC-CSC				FPC			
		40	45	50	55	40	45	50	55
Coal		86.72	86.79	86.85	86.78	86.72	86.74	86.82	86.77
Oil		56.19	56.24	56.27	56.23	56.19	56.20	56.25	56.23
Liquefied petro	Liquefied petroleum gas		43.98	44.01	43.98	43.95	43.96	44.00	43.97
Natural gas		44.79	44.82	44.85	44.81	44.78	44.80	44.84	44.81
DSSAHP	Direct impact	3.35							
	Indirect impact	9.15	9.66	10.21	10.82	9.75	1.31	10.90	11.54
	TEWI	12.50	13.01	13.55	14.16	13.10	13.66	14.24	14.89

5. For DSSAHP using CPC-CSC, as $T_{\rm HWS}^*$ decreases from 55 to 40 °C, $SPF_{\rm ASHP}$ and $SPF_{\rm SWHP}$ significantly increase by 16.7 % and 14.3 %, and seasonal and yearly $SPF_{\rm sys}$ increase by even 17.1 % and 20.5 %. This results from both passive heating and HP heating sectors. On the one hand, low temperature heating allows more heat provision from direct SHW and thus apparently increases system efficiency. On the other hand, generally, the low heating temperature benefits for low condensing temperature and thus high HP efficiency.

CRediT authorship contribution statement

Li Wei Yang: Writing – original draft, Visualization, Methodology,

Investigation, Formal analysis, Data curation, Conceptualization. Jin Huan Pu: Writing – review & editing, Supervision, Project administration, Methodology. Rong Ji Xu: Writing – review & editing, Validation, Resources, Investigation. Tong Yang: Writing – review & editing, Resources, Methodology. Hua Sheng Wang: Writing – review & editing, Supervision, Software, Resources, Project administration, Funding acquisition.

Declaration of competing interest

The authors declare that they have no known competing financial interests or personal relationships that could have appeared to influence

Table 5Economic analysis for DSSAHP using CPC-CSC and FPC based on electricity prices in May 2024.

		Electric water heater	DSSAHP using CPC-CSC				DSSAHP u	DSSAHP using FPC			
Set heating temperature		_	40	45	50	55	40	45	50	55	
Heat provision per year. MWh		11.19	11.18	11.19	11.2	11.19	11.18	11.19	11.2	11.19	
Efficiency / SPF			4.7	4.4	4.2	3.9	4.4	4.1	3.9	3.7	
Electricity consump	Electricity consumption, MWh/year		2.38	2.54	2.67	2.87	2.54	2.73	2.87	3.02	
Initial cost, GBP	collector	0	2160	2160	2160	2160	1880	1880	1880	1880	
initial cost, GDI	tanks	815	2465	2465	2465	2465	2465	2465	2465	2465	
	heater/HPs	3000	6000	6000	6000	6000	6000	6000	6000	6000	
pumps	pumps	0	360	360	360	360	360	360	360	360	
	installation	0	480	480	480	480	480	480	480	480	
	total	3815	11,465	11,465	11,465	11,465	11,185	11,185	11,185	11,185	
Operation cost, GBP)	852.09	172.08	183.97	192.91	207.56	183.81	197.44	207.75	218.78	
Cost saving, GBP/ye	Cost saving, GBP/year		680.01	668.12	659.18	644.53	668.28	654.65	644.34	633.31	
Payback period, year		-	11.25	11.45	11.61	11.87	11.03	11.26	11.44	11.64	

the work reported in this paper.

Acknowledgment

The authors gratefully acknowledge the financial support from the Joint PhD Studentship of China Scholarship Council (CSC) and Queen Mary University of London (201808060459).

Data availability

The authors do not have permission to share data.

References

- [1] Low temperature heating systems, Building Research Establishment, https://www.ncm-pcdb.org.uk/sap/lowtemperatureheating [accessed on June 8th, 2024].
- [2] H. Lund, P.A. Østergaard, T.B. Nielsen, S. Werner, J.E. Thorsen, O. Gudmundsson, A. Arabkoohsar, B.V. Mathiesen, Perspectives on fourth and fifth generation district heating, Energy 227 (2021) 120520.
- [3] District heating, International Energy Agency, https://www.iea.org/reports/district-heating [accessed on June 8th, 2024].
- [4] B. Kilkis, An exergy-based minimum carbon footprint model for optimum equipment oversizing and temperature peaking in low-temperature district heating systems, Energy 236 (2021) 121339.
- [5] S.N. Rabelo, T.F. Paulino, L. Machado, W.M. Duarte, Economic analysis and design optimization of a direct expansion solar assisted heat pump, Sol Energy 188 (2019) 164–174.
- [6] S.N. Rabelo, T.F. Paulino, W.M. Duarte, A.A.T. Maia, L. Machado, Experimental analysis of the influence of the expansion valve opening on the performance of the small size CO2 solar assisted heat pump, Sol Energy 190 (2019) 255–263.
- [7] X.Q. Kong, P.L. Sun, K.L. Jiang, S.D. Dong, Y. Li, J.B. Li, A variable frequency control method and experiments of a direct-expansion solar-assisted heat pump system, Sol Energy 176 (2018) 572–580.
- [8] L.W. Yang, R.J. Xu, N. Hua, Y. Xia, W.B. Zhou, T. Yang, Belyayev Ye, Wang HS, Review of the advances in solar-assisted air source heat pumps for the domestic sector, Energy Convers, Manage 247 (2021) 114710.
- [9] L.W. Yang, N. Hua, J.H. Pu, Y. Xia, W.B. Zhou, R.J. Xu, T. Yang, Belyayev Ye, Wang HS, Analysis of operation performance of three indirect expansion solar assisted air source heat pumps for domestic heating, Energy Convers, Manage 252 (2022) 115061.
- [10] K. Kaygusuz, Experimental and theoretical investigation of a solar heating system with heat pump, Renew Energy 21 (2000) 79–102.
- [11] Y. Yerdesh, Z. Abdulina, A. Aliuly, Y. Belyayev, M. Mohanraj, A. Kaltayev, Numerical simulation on solar collector and cascade heat pump combi water heating systems in Kazakhstan climates, Renew Energy 145 (2020) 1222–1234.
- [12] G.D. Qiu, X.H. Wei, Z.F. Xu, W.H. Cai, A novel integrated heating system of solar energy and air source heat pumps and its optimal working condition range in cold regions, Energy Convers Manage 174 (2018) 922–931.
- [13] L.W. Yang, Y. Li, T. Yang, H.S. Wang, Low temperature heating operation performance of a domestic heating system based on indirect expansion solar assisted air source heat pump, Sol Energy 244 (2022) 134–154.
- [14] J. Vega, C. Cuevas, Parallel vs series configurations in combined solar and heat pump systems: a control system analysis, Appl Therm Eng 166 (2020) 114650.

- [15] W. He, X.Q. Hong, X.D. Zhao, X.X. Zhang, J.C. Shen, J. Ji, Operational performance of a novel heat pump assisted solar façade loop-heat-pipe water heating system, Appl Energy 146 (2015) 371–382.
- [16] S.M. Buker, S.B. Riffat, Build-up and performance test of a novel solar thermal roof for heat pump operation, Int J Ambient Energy 38 (2017) 365–379.
- [17] C. Treichel, C.A. Cruickshank, Energy analysis of heat pump water heaters coupled with air-based solar thermal collectors in Canada and the United States, Energy 221 (2021) 119801.
- [18] B. Wei, Y.Z. Wang, Z.J. Liu, B.X. Liu, Optimization study on a solar-assisted air source heat pump system with energy storage based on the economics method, Int J Energy Res 44 (2020) 2023–2036.
- [19] R.J. Xu, Y.Q. Zhao, H. Chen, Q. Wu, L.W. Yang, H.S. Wang, Numerical and experimental investigation of a compound parabolic concentrator-capillary tube solar collector, Energy Convers Manage 204 (2020) 112218.
- [20] R. Dickes, V. Lemort, S. Quoilin, Semi-empirical correlation to model heat losses along solar parabolic trough collectors Proceedings of ECOS 2015–28th International Conference on Efficiency, Cost, Optimization, Simulation and Environmental Impact of Energy Systems, ECOS, Pau, France, 2015.
- [21] L.W. Yang, R.J. Xu, W.B. Zhou, Y. Li, T. Yang, H.S. Wang, Investigation of solar assisted air source heat pump heating system integrating compound parabolic concentrator-capillary tube solar collectors, Energy Convers Manage 277 (2023) 116607
- [22] R. Dott, M.Y. Haller, J. Ruschenburg, F. Ochs, J. Bony, The Reference Framework for System Simulations of the IEA SHC Task 44 / HPP Annex 38—Part B: Buildings and Space Heat Load, A technical report of subtask C—Report C1 Part B, International Energy Agency (2013).
- [23] Charted Institute of Plumbing and Heating Engineering, https://www.ciphe.org. uk/consumer/safe-water-campaign/hot-water-scalds/ [accessed on June 22nd, 2024].
- [24] L. Aye, W.W.S. Charters, C. Chaichana, SOLAR HEAT PUMP SYSTEMS FOR DOMESTIC HOT WATER, Sol Energy 73 (3) (2002) 169–175.
- [25] Technology-specific Cost and Performance Parameters, Intergovernmental Panel on Climate Change, https://www.ipcc.ch/site/assets/uploads/2018/02/ipcc_wg3_ ar5_annex-iii.pdf#page=7 [accessed on June 22nd, 2024].
- [26] K. Bakirci, B. Yuksel, Experimental thermal performance of a solar source heatpump system for residential heating in cold climate region, Appl Therm Eng 31 (2011) 1508–1518.
- [27] H. Li, H.X. Yang, Potential application of solar thermal systems for hot water production in Hong Kong, Appl Energy 86 (2009) 175–180.
- [28] https://www.statista.com/statistics/589765/average-electricity-prices-uk/, [accessed on August 14th, 2024].
- [29] https://www.screwfix.com/c/heating-plumbing/boilers/cat6660001? boilertype=combi#category=cat6660001&boilertype=heat_only [accessed on August 14th, 2024].
- [30] https://www.screwfix.com/p/rm-cylinders-500ltr-indirect-unvented-hot-waterstorage-cylinder/8141p [accessed on August 14th, 2024].
- [31] https://www.machinemart.co.uk/categories/?search=Electric+ Pump&Category=Water+Pumps&Max%20Head=14+m [accessed on August 14th, 2024].
- [32] https://www.heiz24.de/Flat-plate-collector-Sunex-type-AMP-251-250qm-New? curr=EUR&gclid=EAIaIQobChMIicej1bzRgIVpWLmCh3Q0wEEEAQYASABEgKuzfD_BwE [accessed on August 14th, 2024].
- [33] https://www.bimblesolar.com/solar-thermal-30-tube [accessed on August 14th, 2024]].
- [34] Committee on Climate Change, The Sixth Carbon Budget The UK's path to Net Zero, 2020, https://www.theccc.org.uk/publication/sixth-carbon-budget/.
- [35] Plumber Costs: 2023 Call Out Charges & Hourly Prices UK, https://tradesmencosts. co.uk/plumbers/ [accessed on August 14th, 2024].